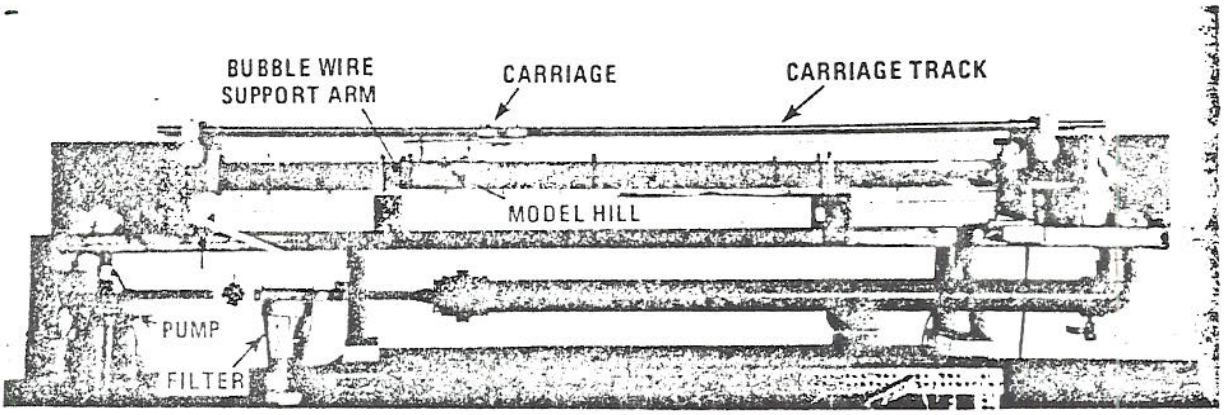

(A) SMALL WATER CHANNEL/STRATIFIED TOWING TANK.

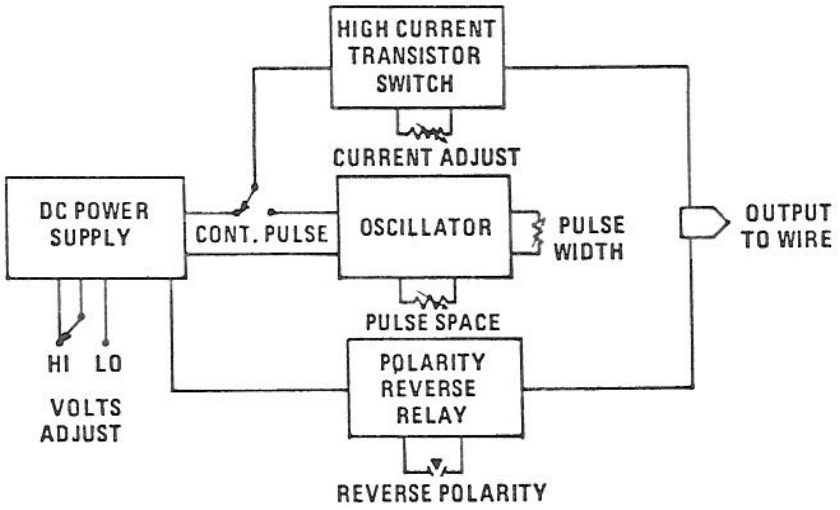

(B) SCHEMATIC DIAGRAM OF CURRENT SOURCE FOR GENERATING HYDROGEN BUBBLES.

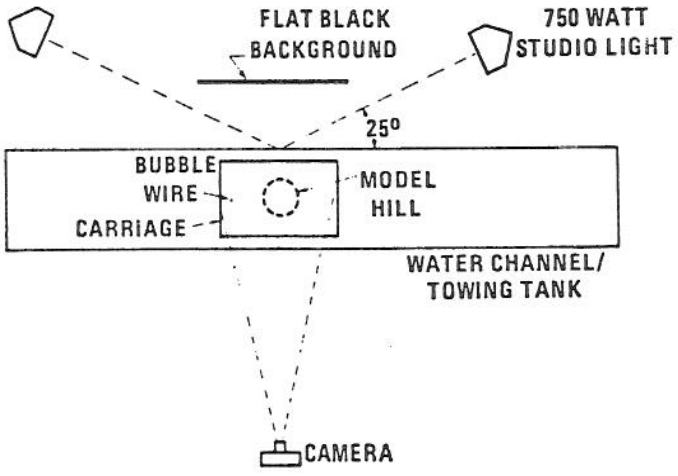

(C) PLAN VIEW OF SET-UP FOR PHOTOGRAPHING HYDROGEN BUBBLES.

Figure 9 Hydrogen bubble apparatus for flow visualization in water channels

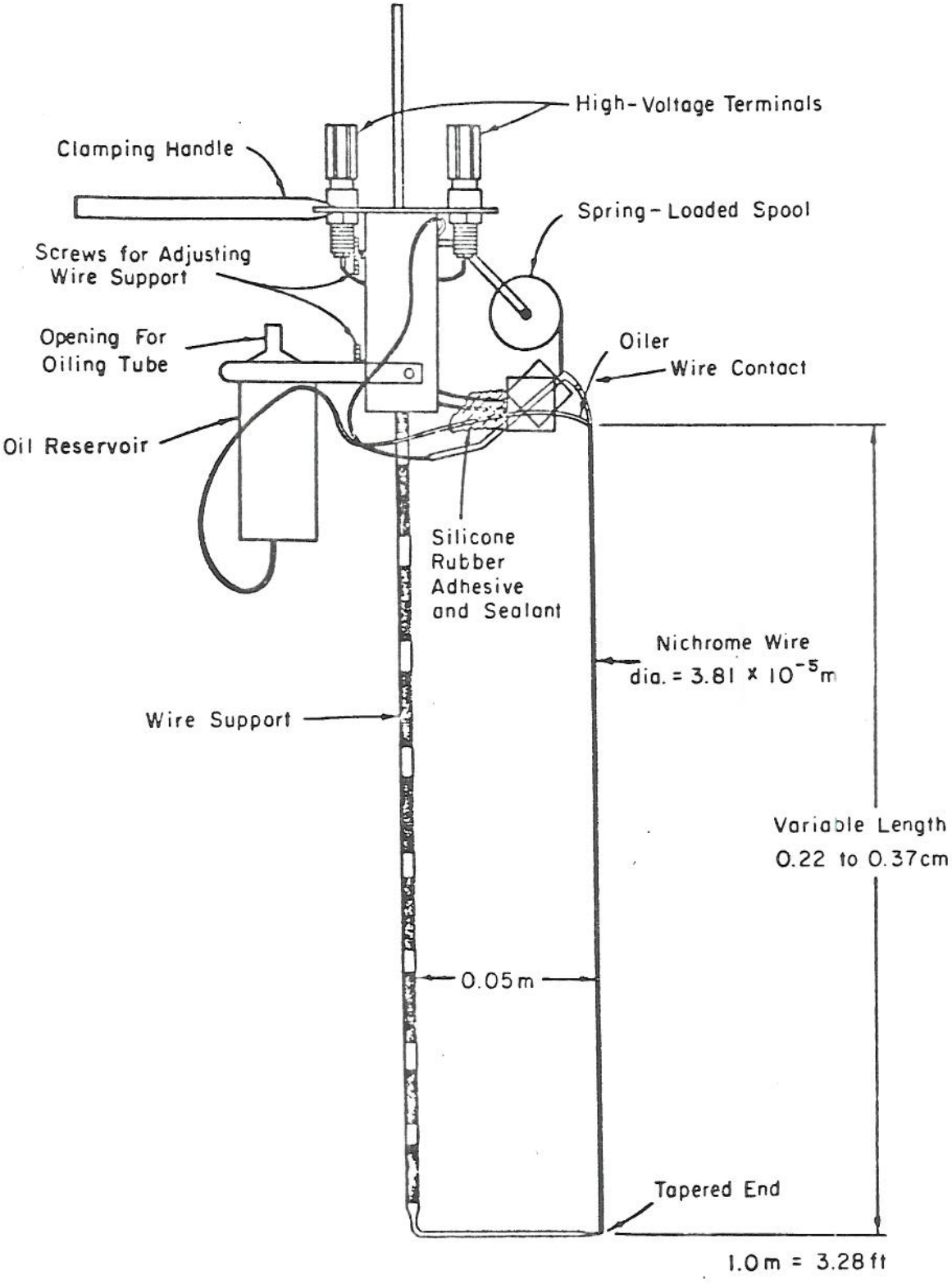

Figure 10 Details of a smoke-wire probe used to obtain airflow velocities for barostromatic model airflow (Orgill et al., 1971a)

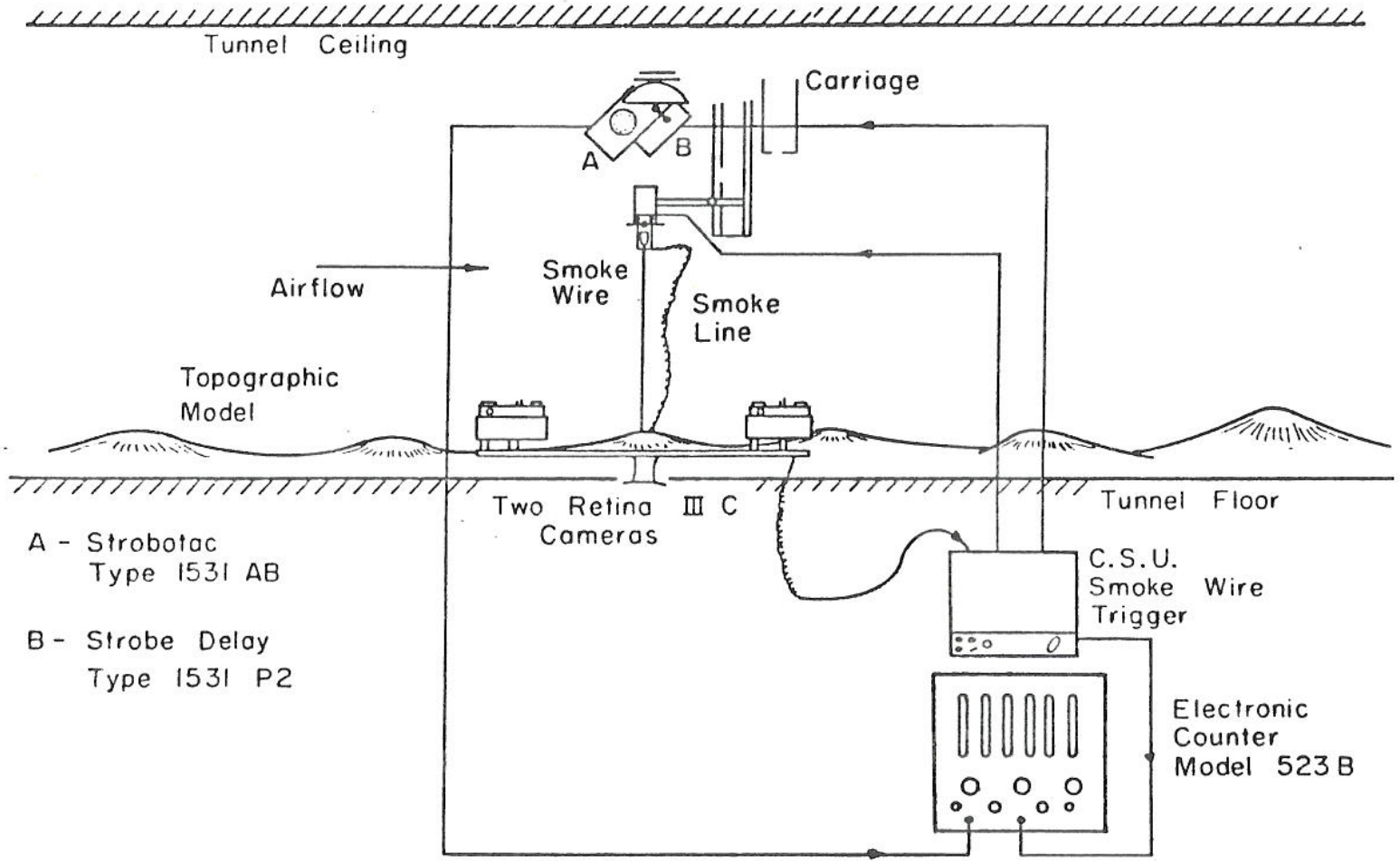

Figure 11 Laboratory experimental arrangement for obtaining airflow velocity measurements by the stereo two-camera smoke-wire method (Orgill et al., 1971a)

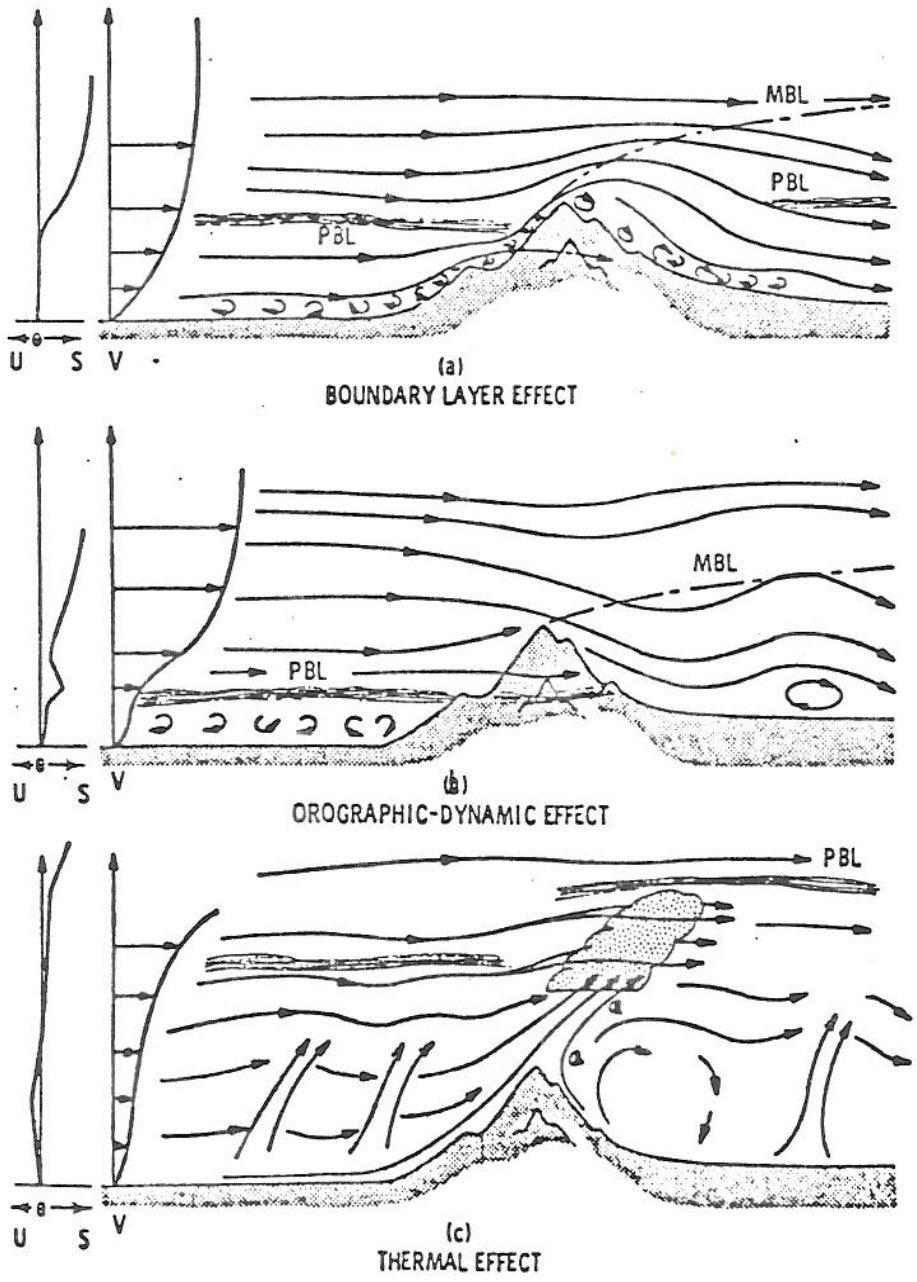

Figure 12 Methods in which terrain features affect atmospheric motions (Drake et al., 1977)

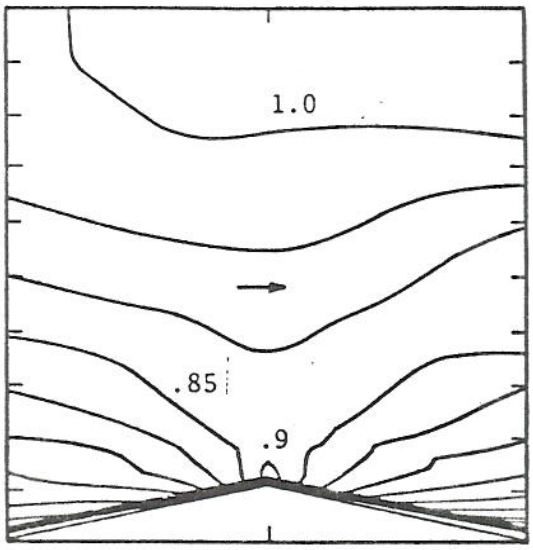

a. Mean longitudinal velocity, $\Delta u/\bar{u}_o$ (δ) = .05

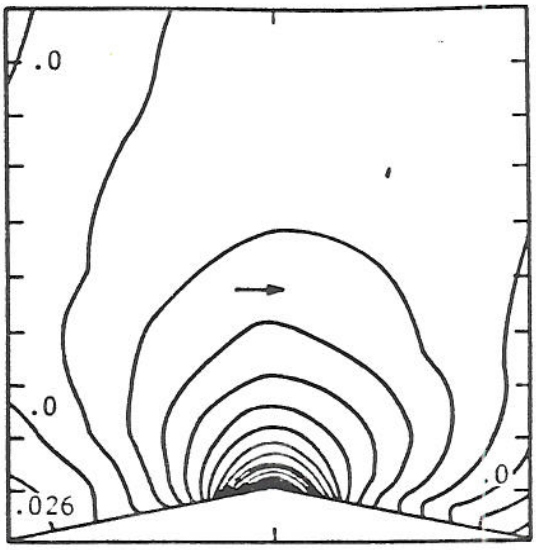

b. Static pressure, ΔC_p = .026

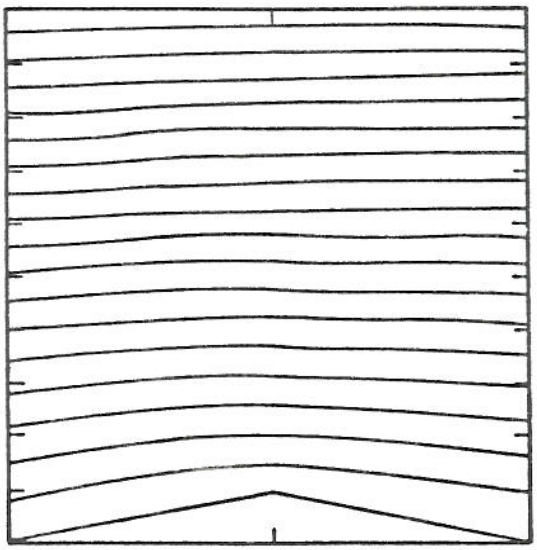

c. Streamlines

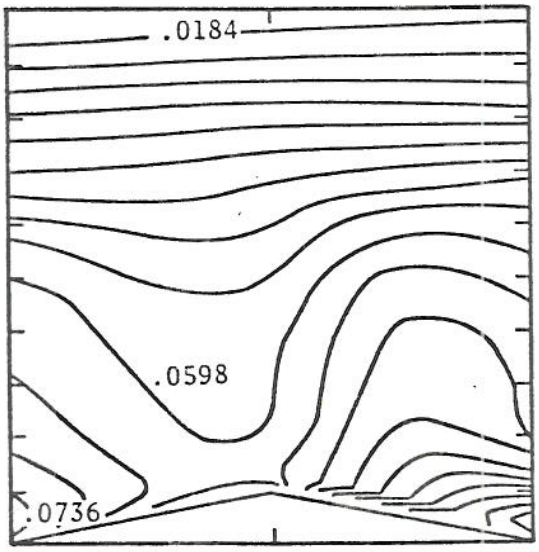

d. Longitudinal turbulence intensity, $\Delta u'/\bar{u}_o$ (δ) = .0046

Figure 13 Contours of flow characteristics over a triangular ridge, h/L = 1/6 (Meroney et al., 1978b)

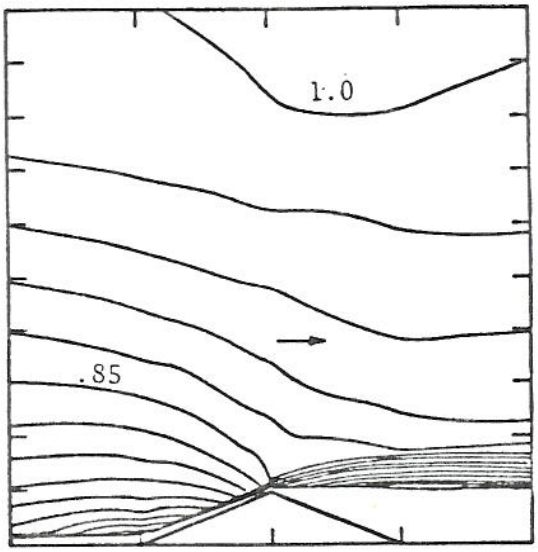

a. Mean longitudinal velocity, $\Delta u/\bar{u}_o$ $(\delta) = 0.5$

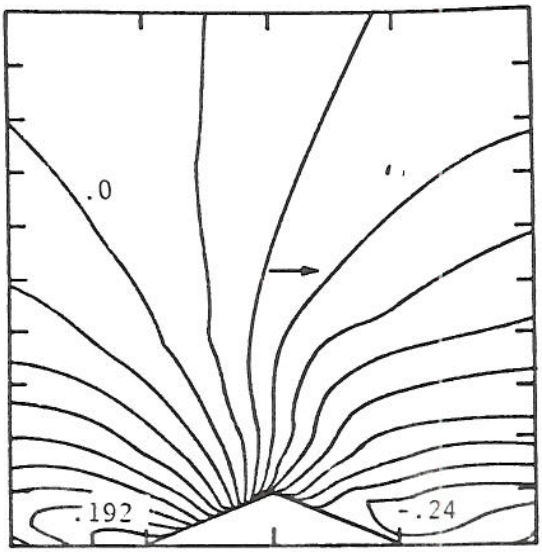

b. Static pressure, $\Delta C_p = 0.27$

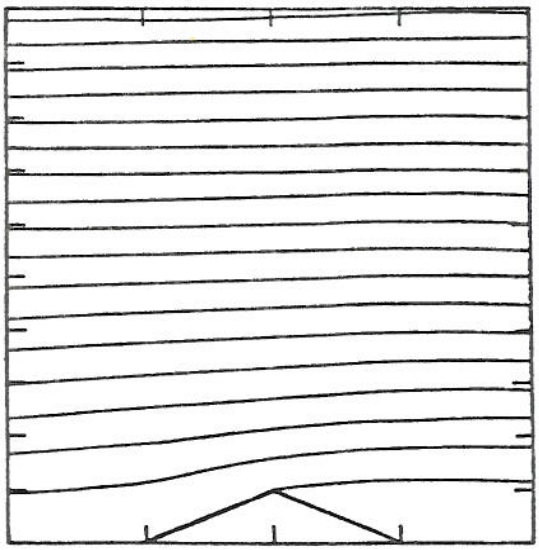

c. Streamlines

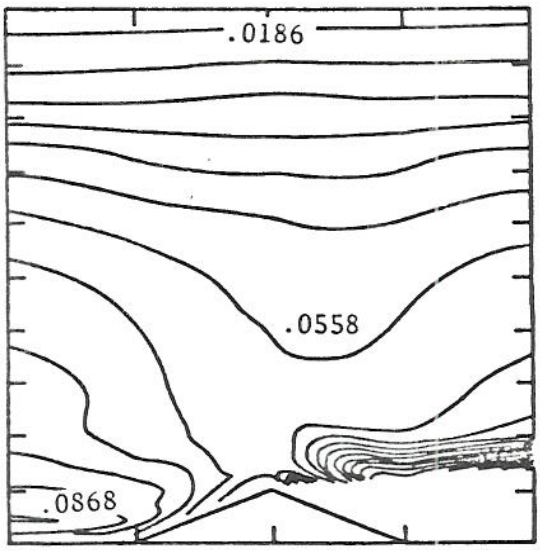

d. Longitudinal turbulence intensity, $\Delta u'/\bar{u}_o$ $(\delta) = .0062$

Figure 14 Contours of flow characteristcs over a triangular ridge, h/L = 1/2 (Meroney et al., 1978b)

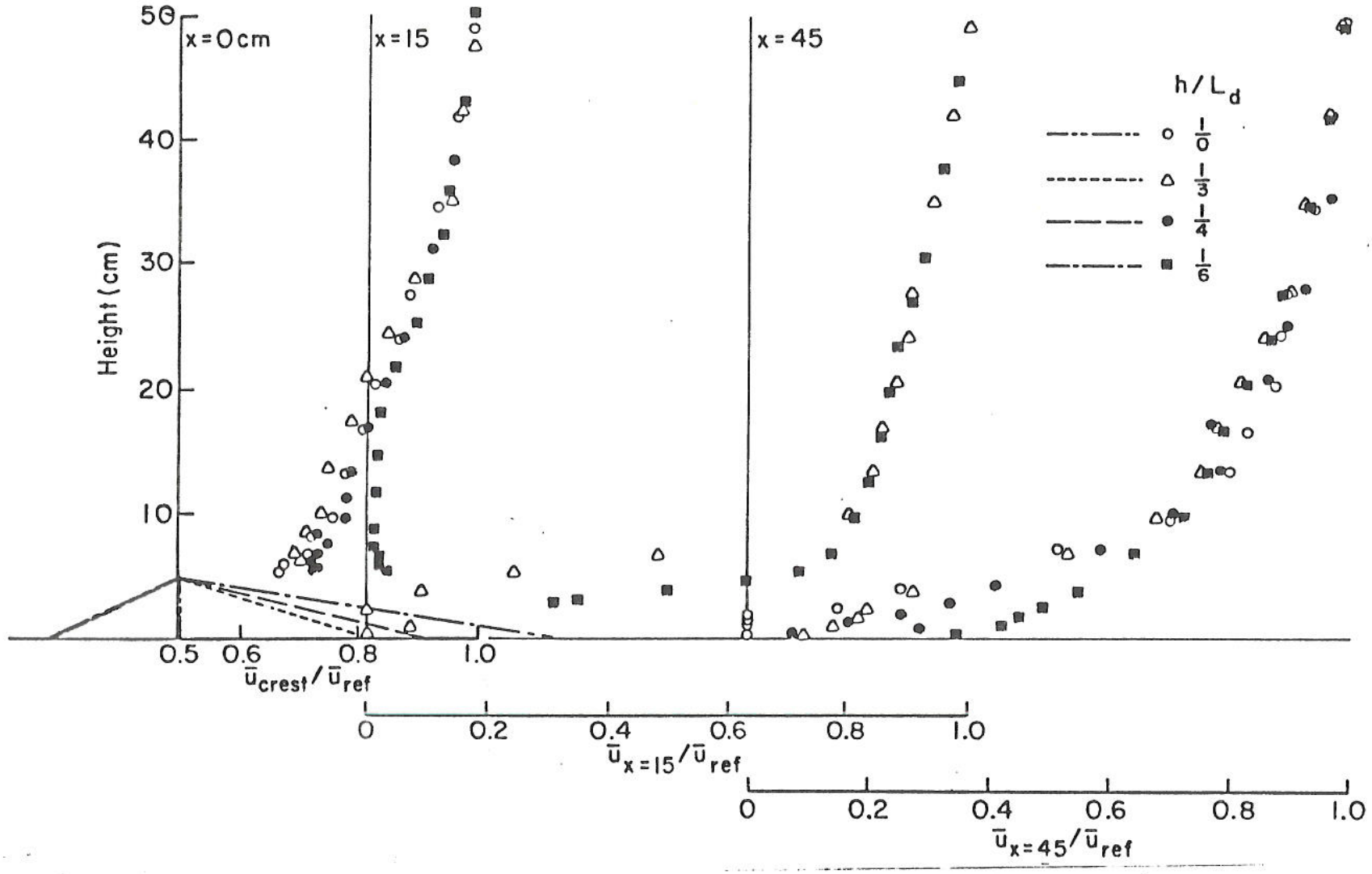

Figure 15 Mean velocity profiles downwind of a triangular hill h/L_u = 0.5 and h/L_d = 1, 0.33, 0.25, 0.17 (Bouwmeester et al., 1978)

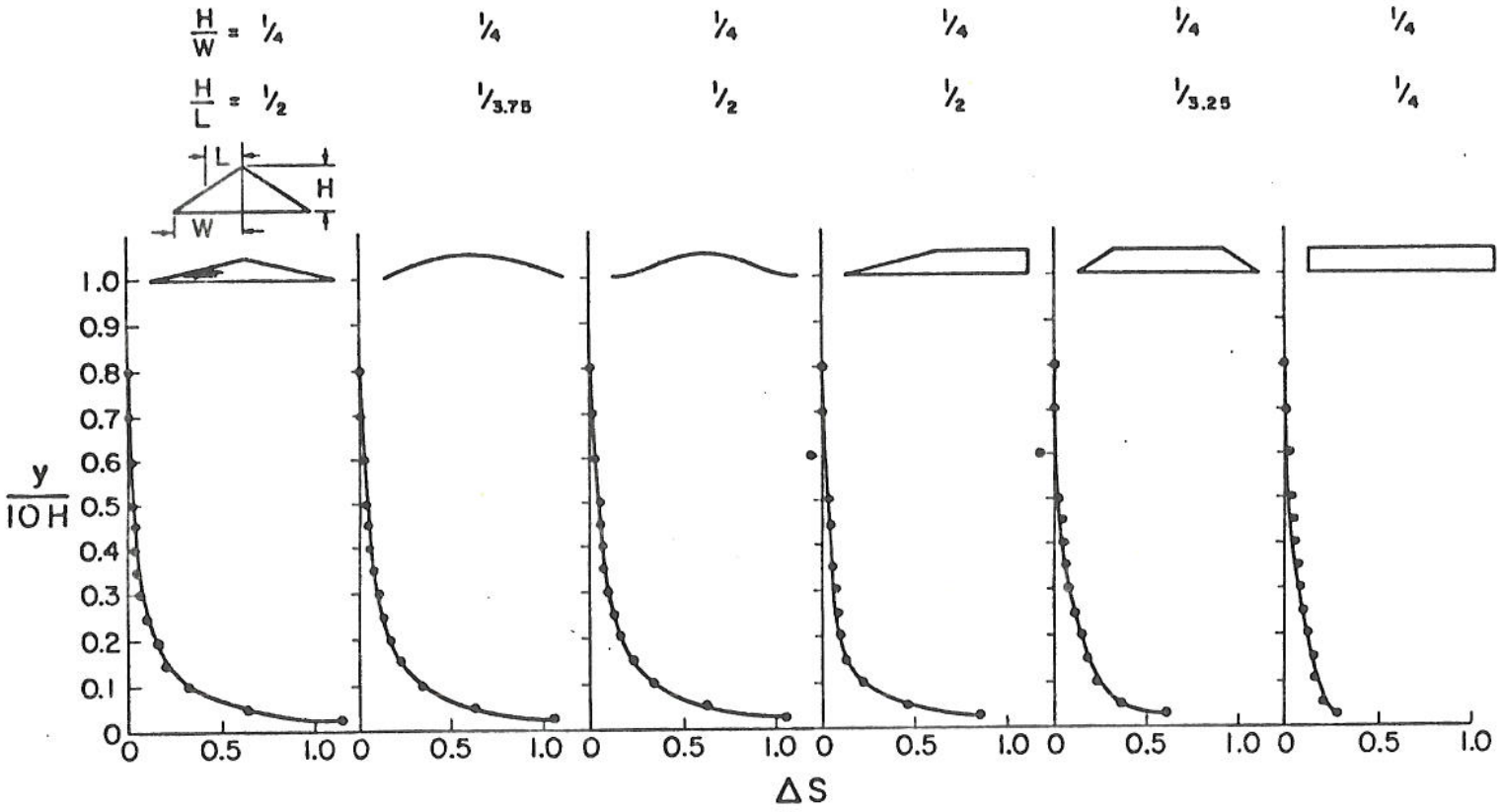

Figure 16 Velocity speedup between approach flow and crest over different hill shapes (Rider and Sandborn, 1977)

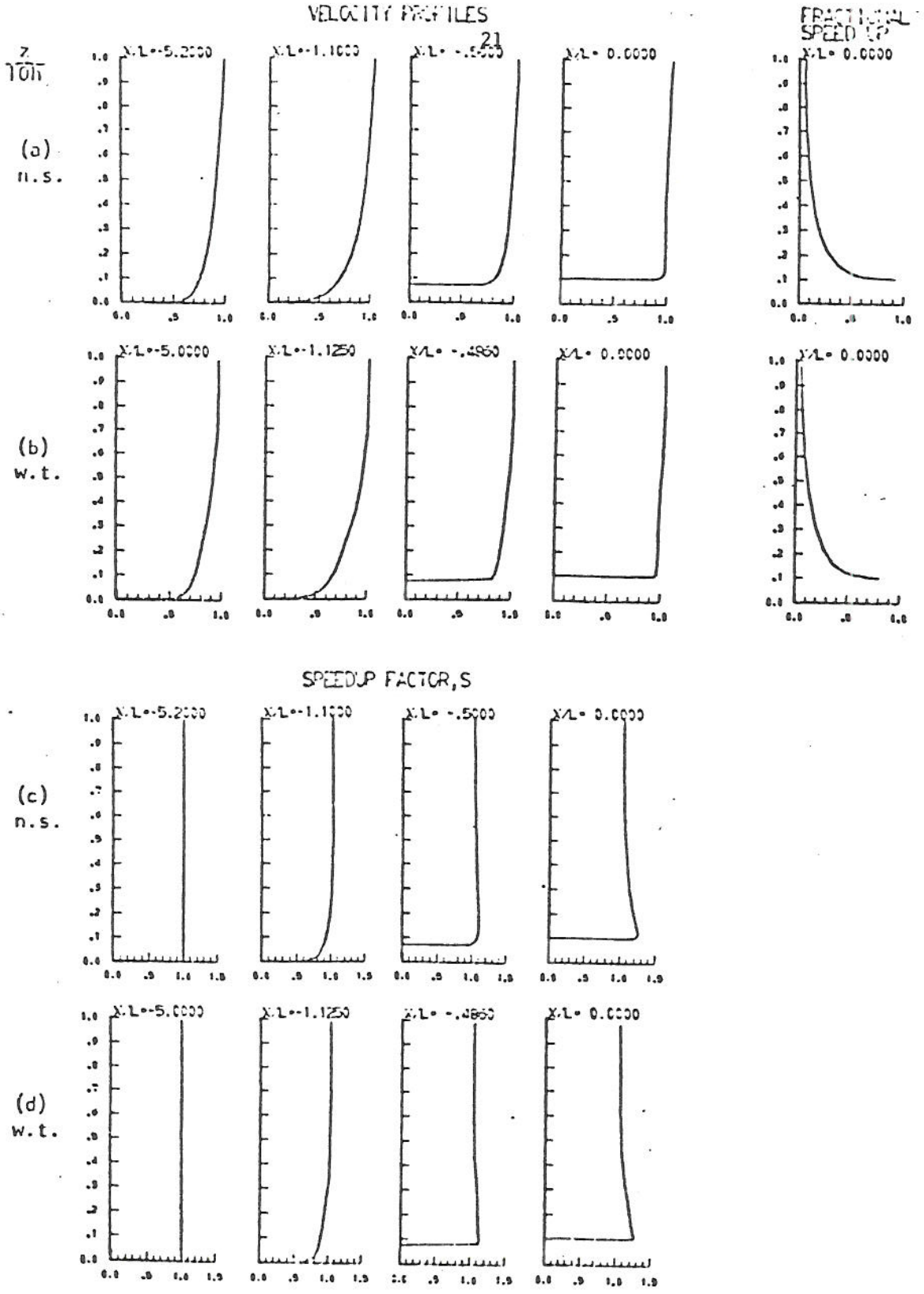

Figure 17 Comparison between wind tunnel (w.t.) and numerical simulation (n.s.) of velocities over a 1:4 sinusoidal hill. L is half width of hill. (Derickson and Meroney, 1977)

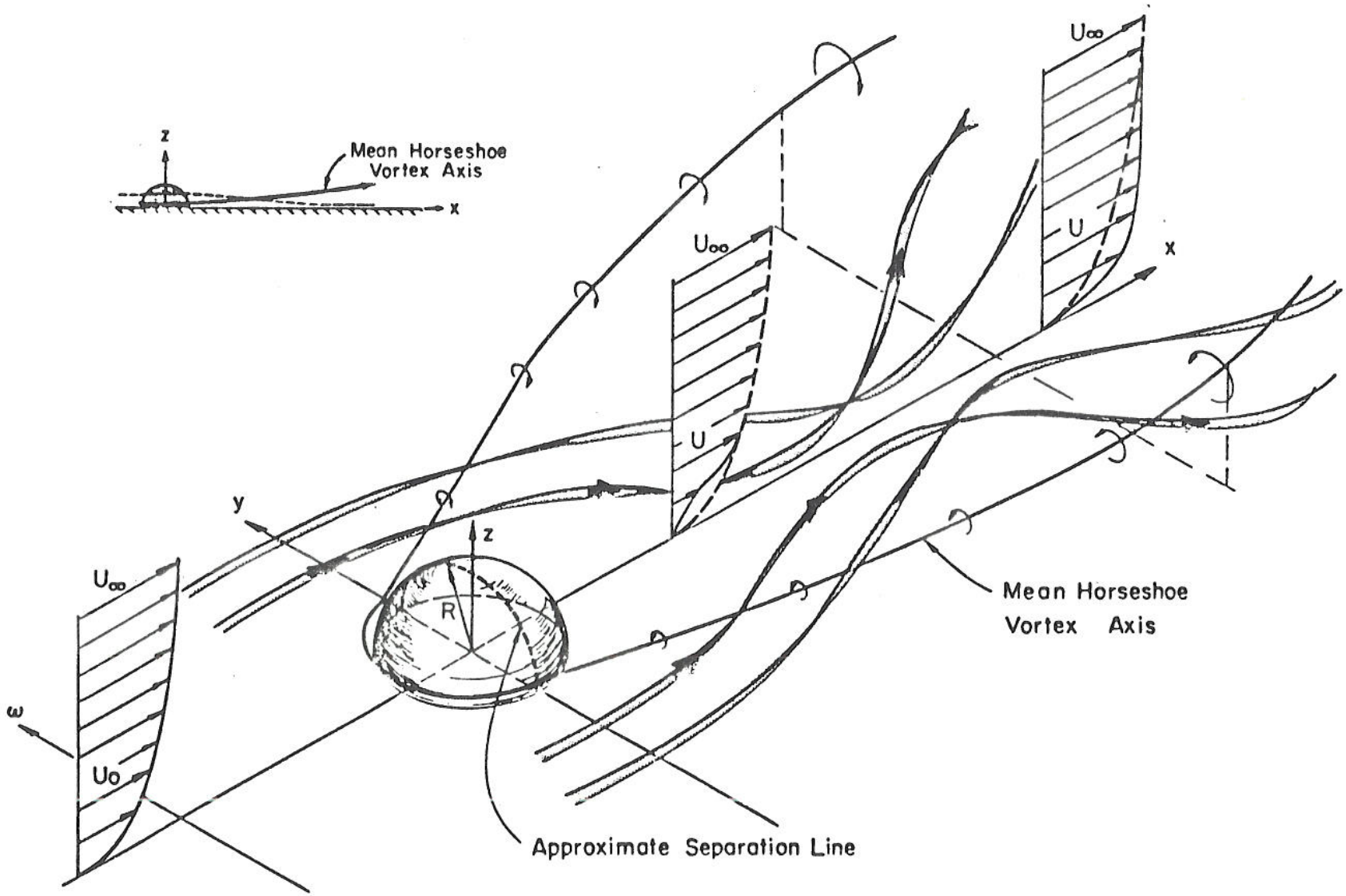

Figure 18 Schematic of the vortex containing wake produced by a hemisphere (Hansen and Cermak, 1975)

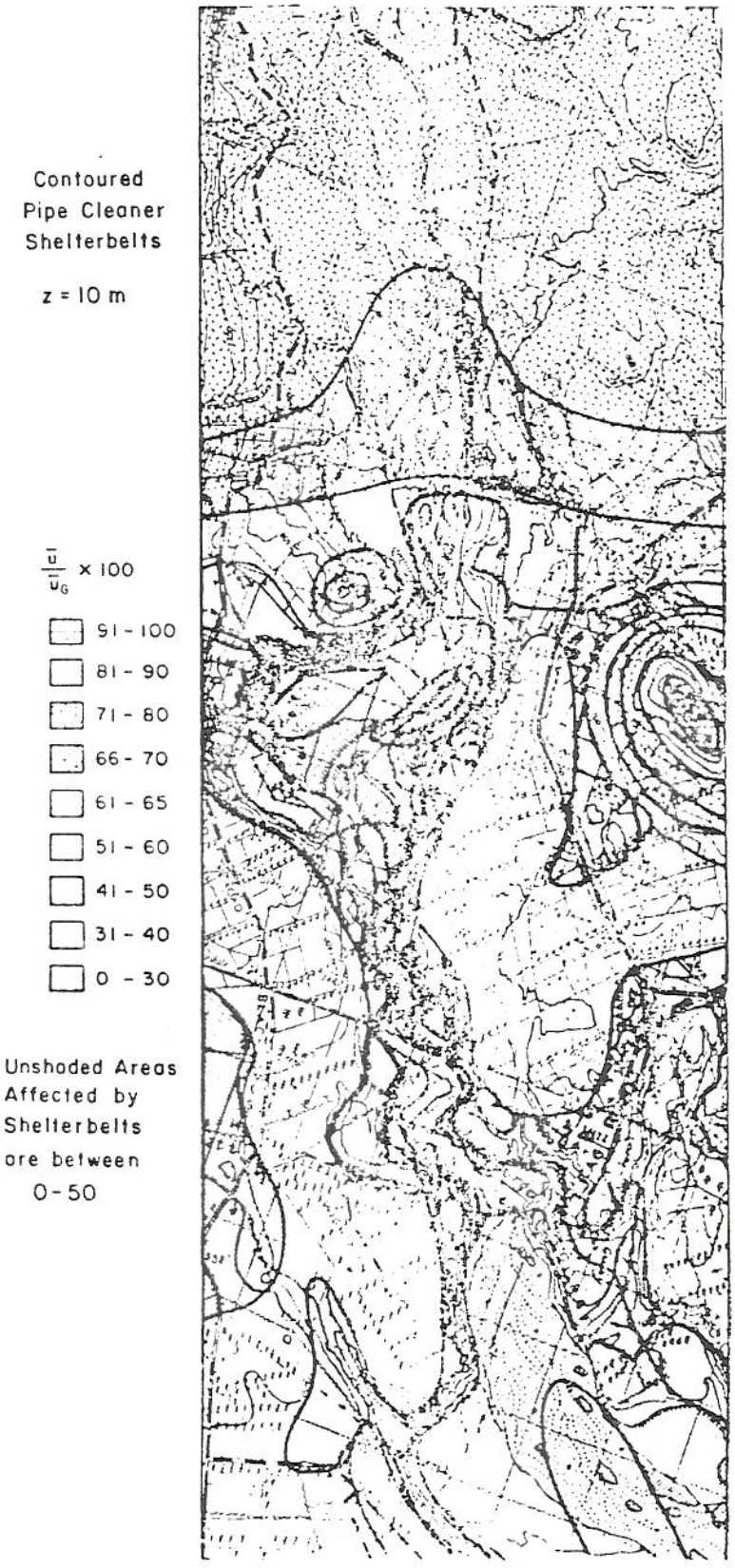

Figure 19 Horizontal isotachs, contoured model with tree shelterbelts at a height of 10M (Meroney et al., 1978)

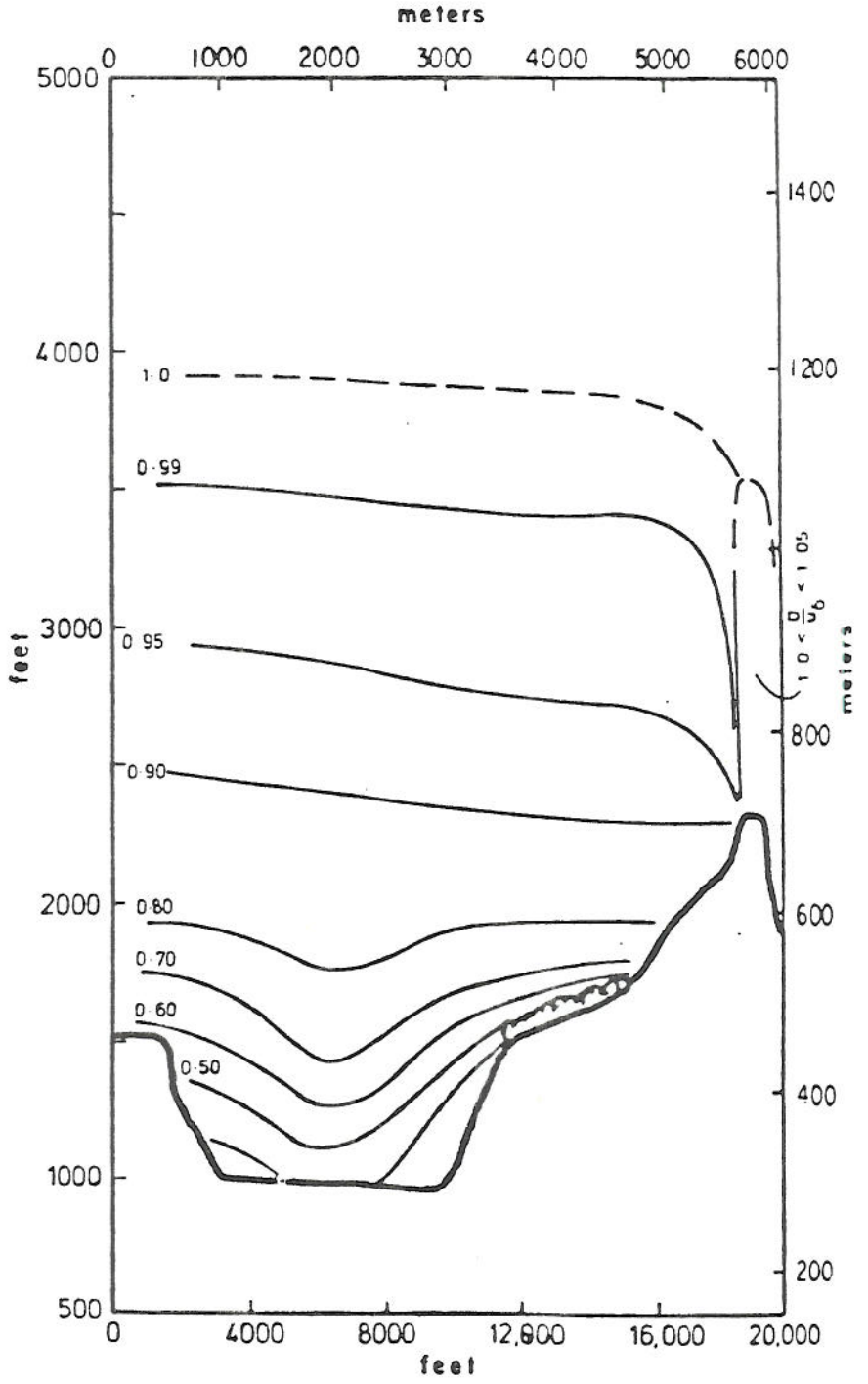

Figure 20 Vertical section of isotachs over Rakaia Gorge contoured model with shelterbelts (Meroney et al., 1978a)

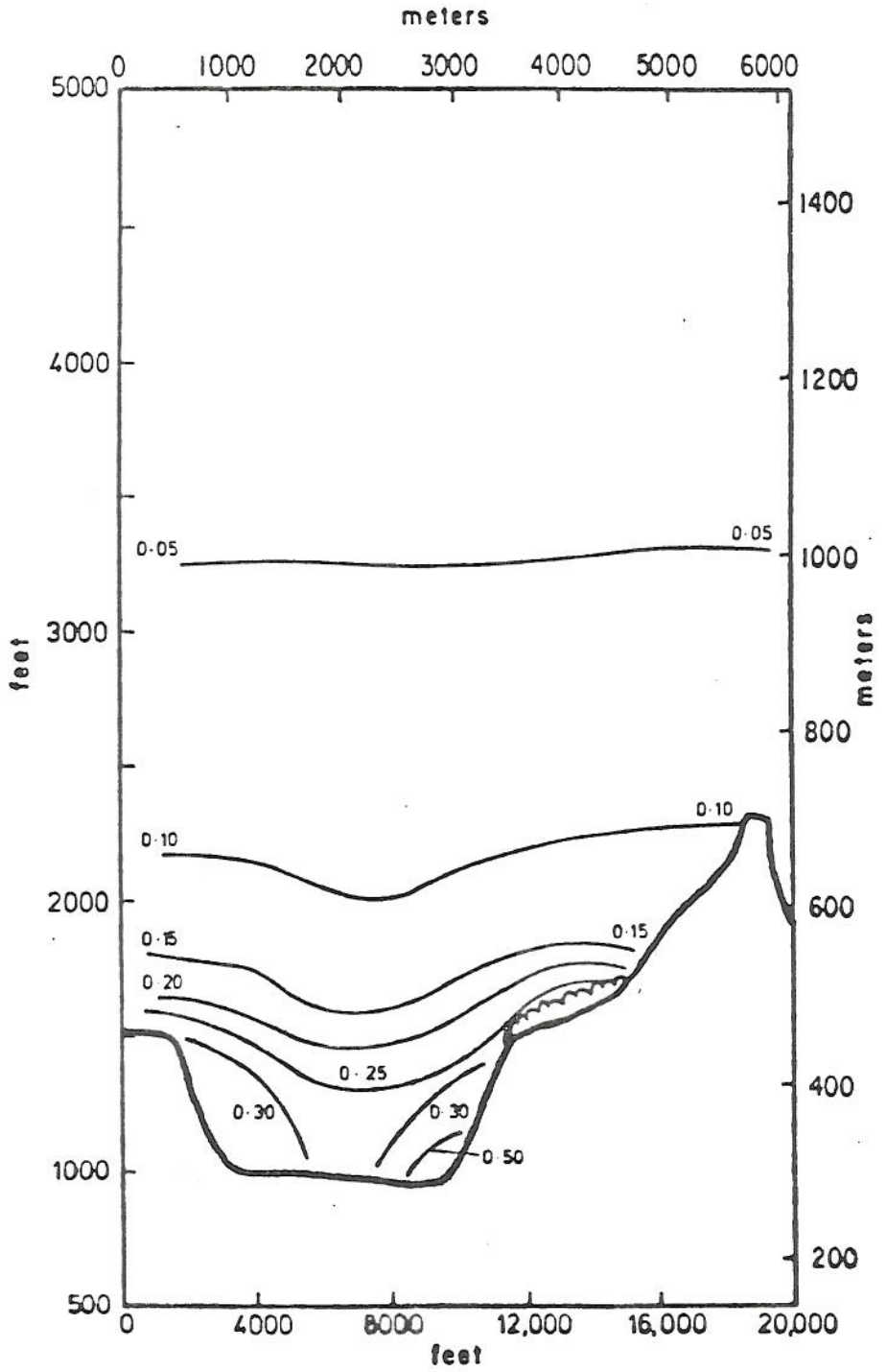

Figure 21 Vertical section of isoturbs over contoured Rakaia Gorge model with shelterbelts (Meroney et al., 1978a)

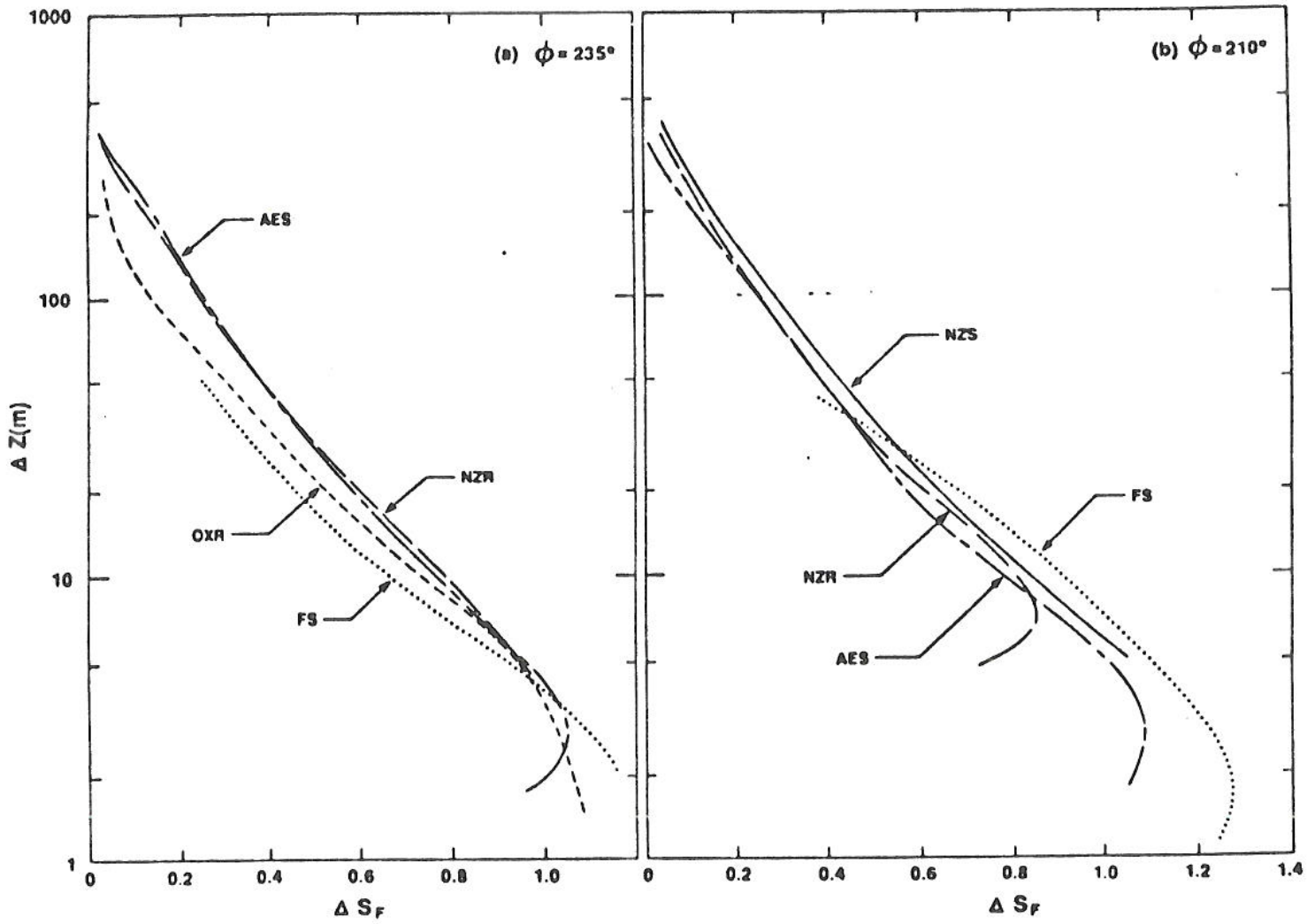

Figure 22 Vertical profiles of mean speed and speedup at the hilltop location for two wind directions in wind-tunnel and full-scale flows. (Teunissen et al., 1987)

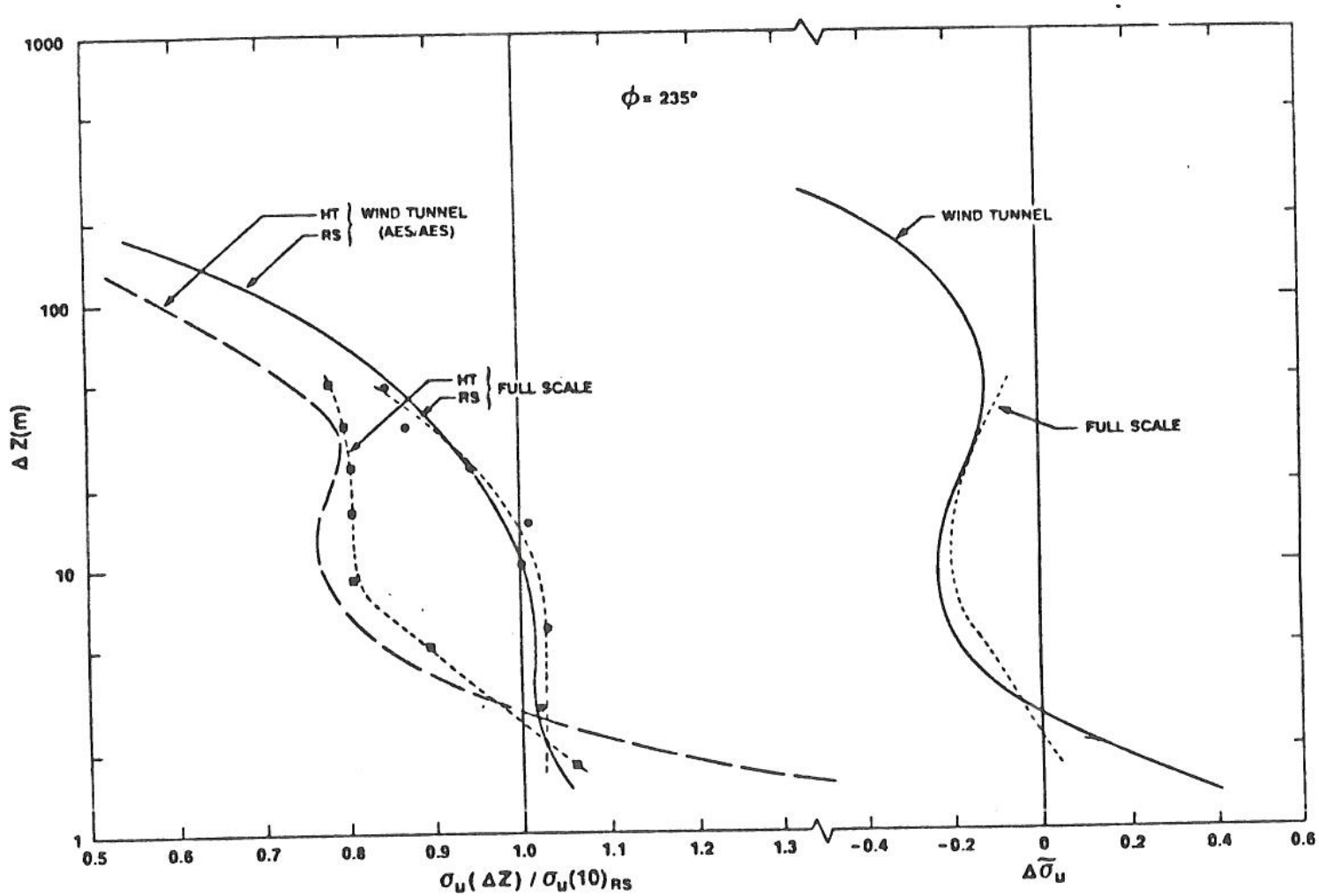

Figure 23 Vertical profiles of σ_u and $\Delta\sigma_u$ at the hill top (HT) and reference location (RS) in wind-tunnel and full-scale flows for ϕ = 235 . (Teunissen et al., 1987)

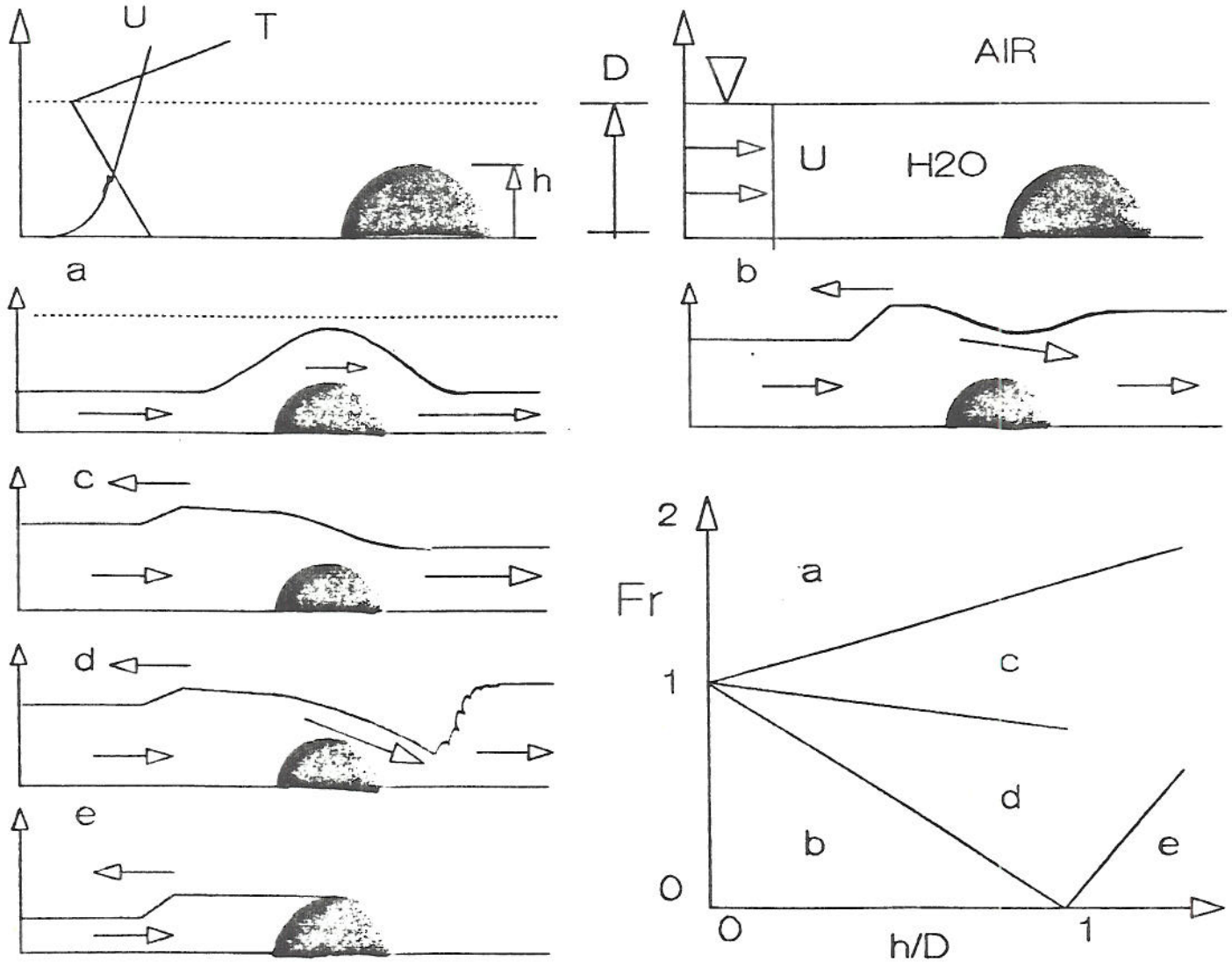

Figure 24 Domains of stratified flow behavior over surface-mounted obstacles as a function of flow-depth Froude number and obstacle to depth ratio

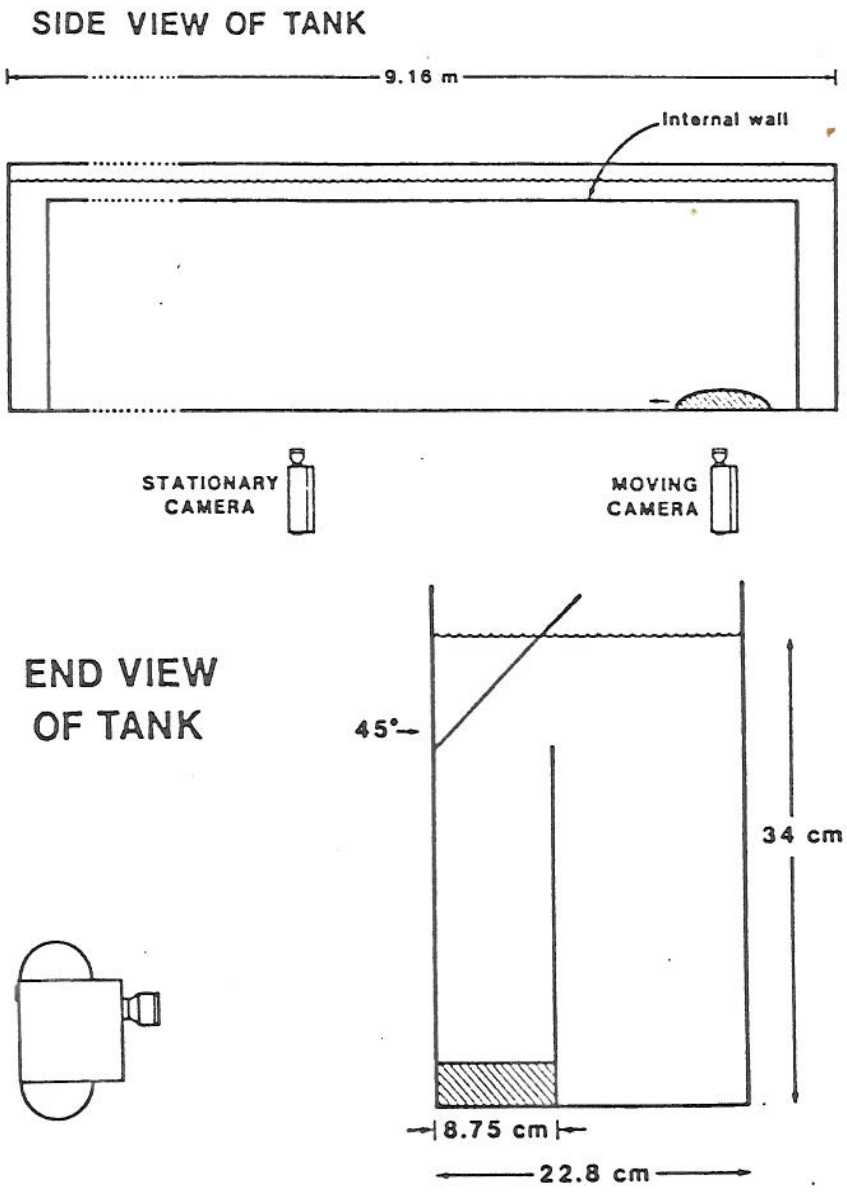

Figure 25 Schematic arrangement of baffles in a water filled towing tank to simulate an infinite depth flow (Baines and Hoinka, 1985)

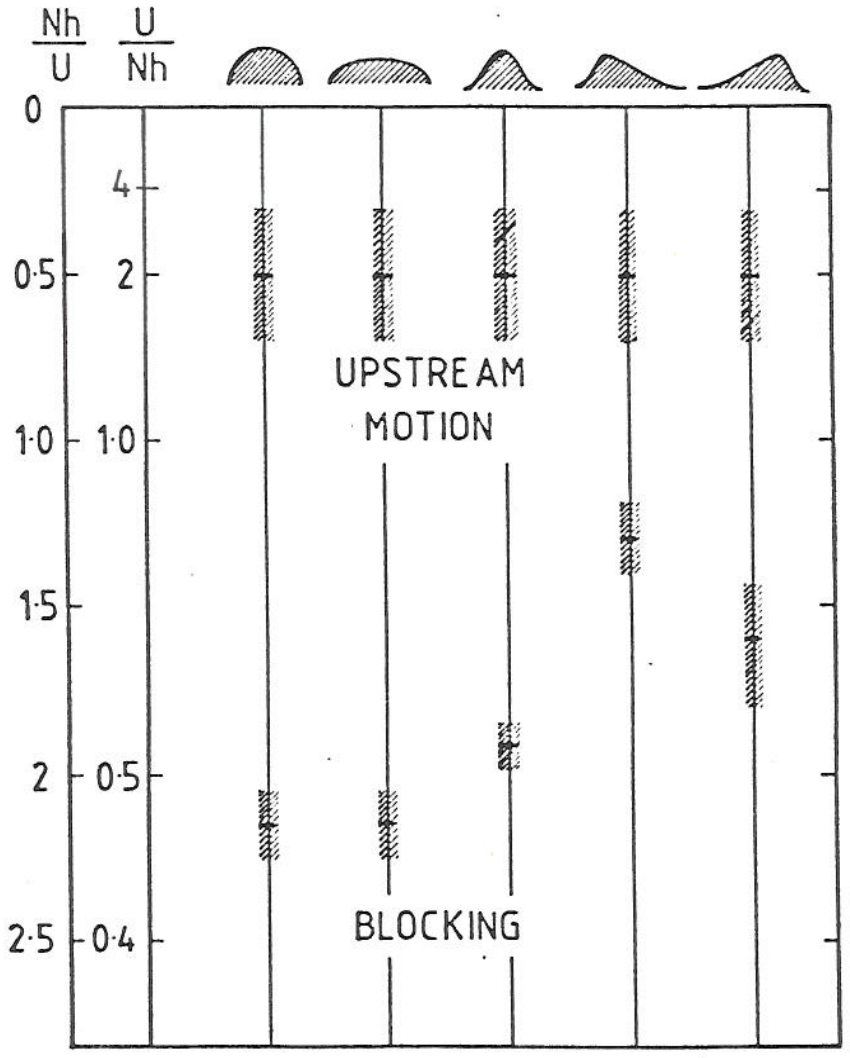

Figure 26 Criteria for the presence of columnar upstream motion and upstream blocking in terms of Nh/U for a range of surface mounted obstacle shapes. Hatched regions denote error bars. (Baines and Hoinka, 1985)

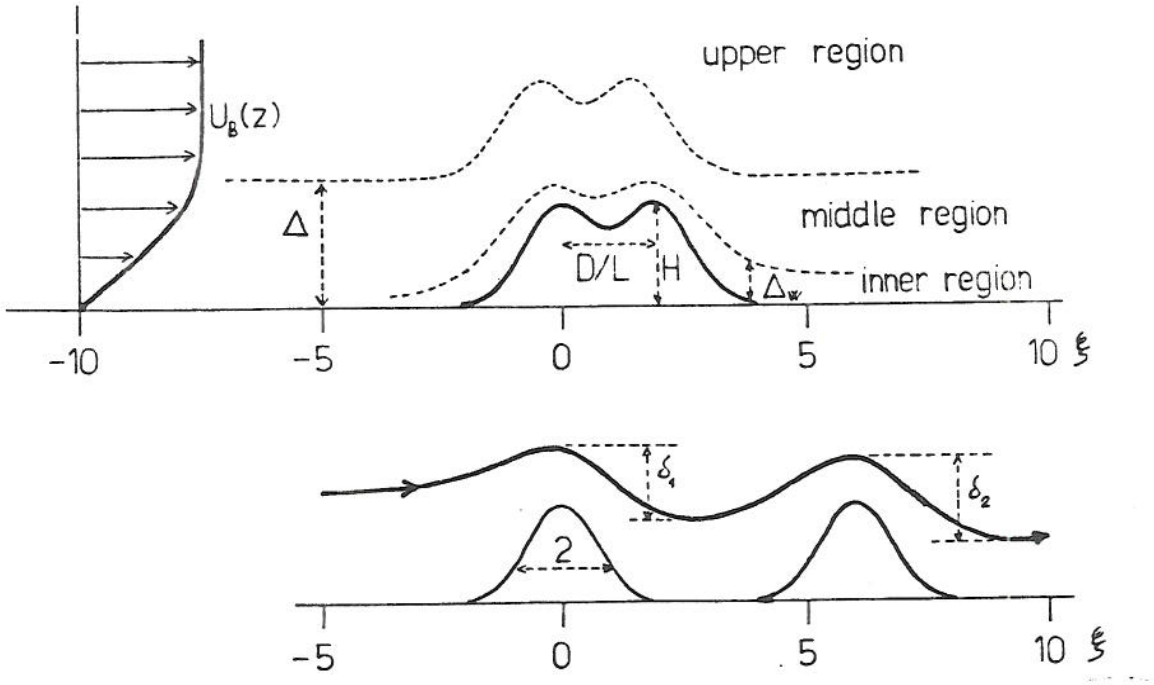

Figure 27 Sketch of stably stratified flow over two humps where the surface height is equivalent to the sum of their separate heights, two spacings (Tampieri and Hunt, 1984)

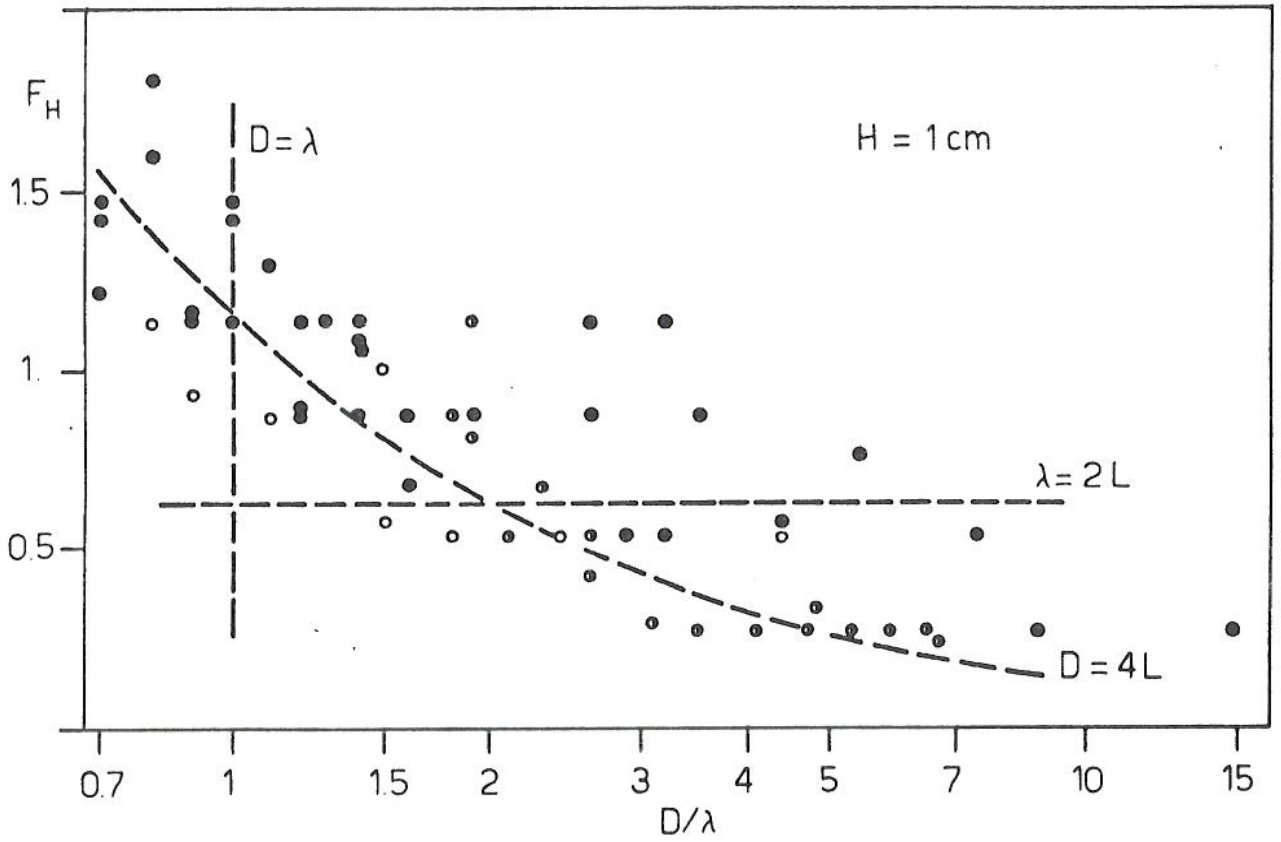

Figure 28 Water channel experiments performed with obstacles 1 cm high. Full symbols correspond to good penetration; open symbols to no penetration; half-filled symbols to inter-mediate cases (Tampieri and Hunt, 1984)

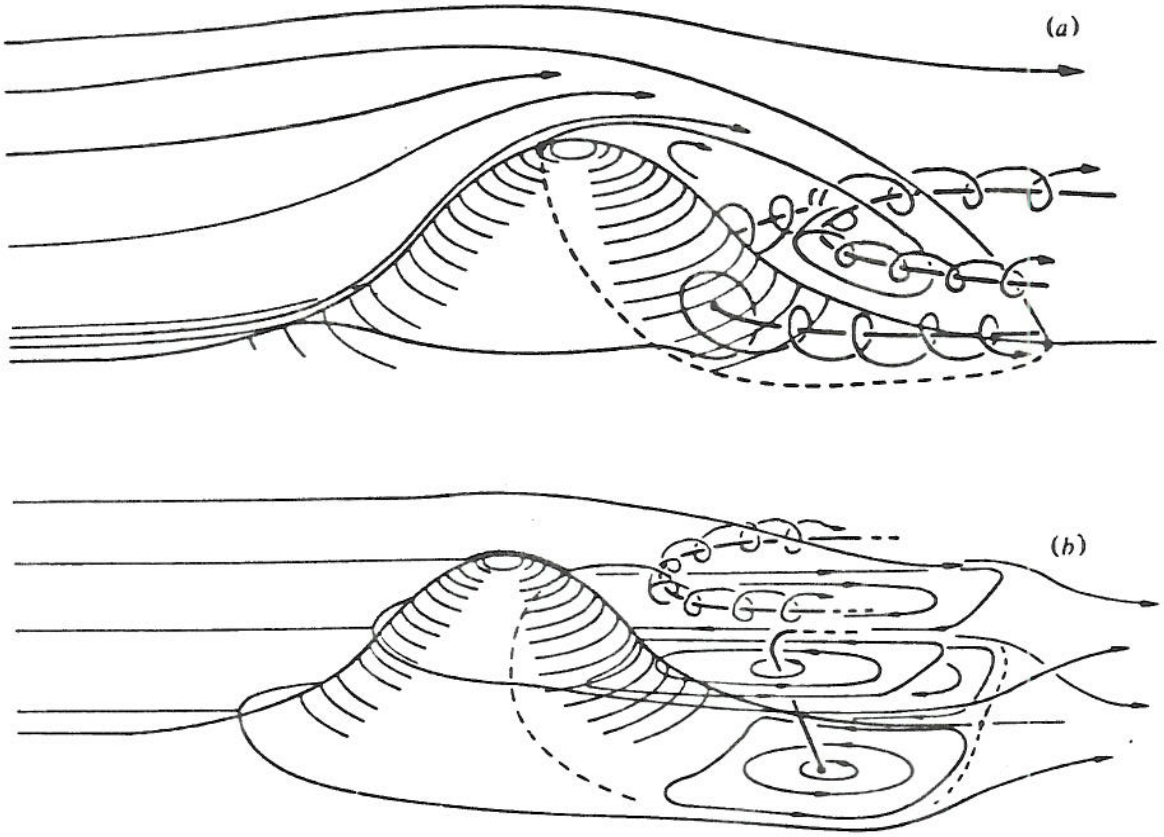

Figure 29 Schematic of dividing streamline concept for stratified flow over hills (Hunt and Snyder 1980)

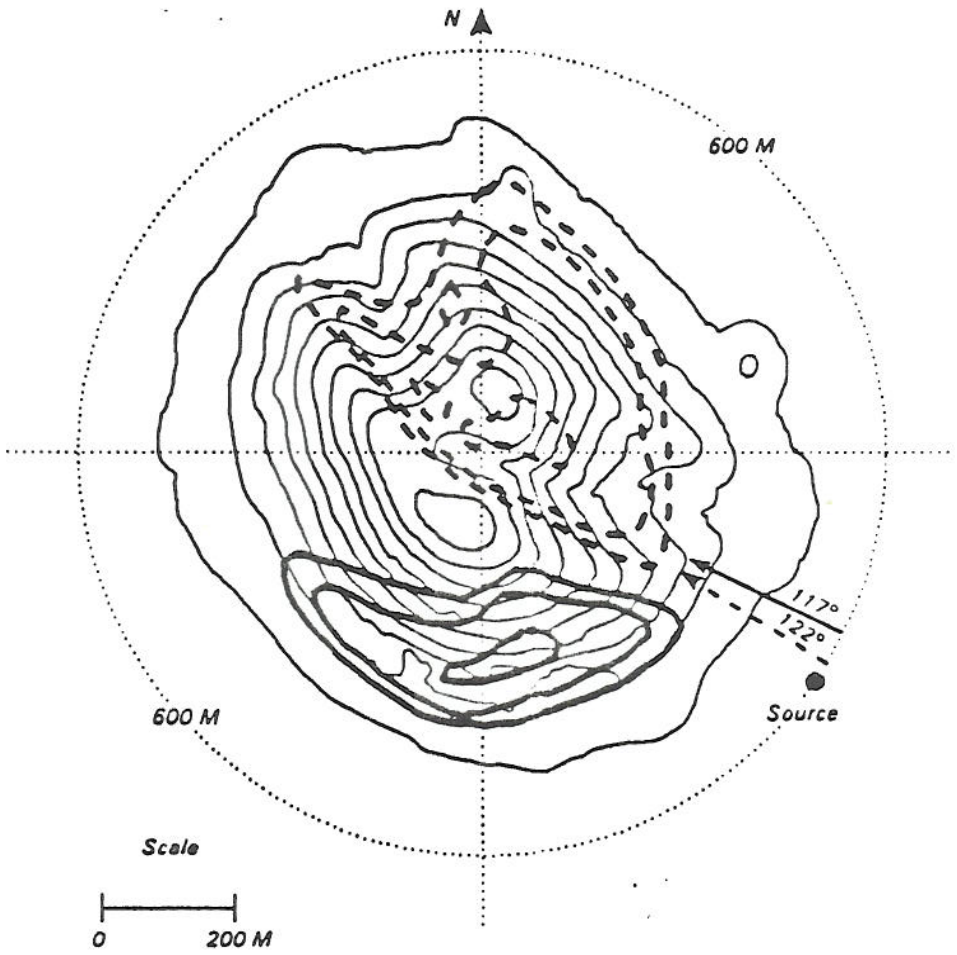

Concentration distributions measured during individual tows of CCB with H_s/h=0.31 and H_D/h=0.38; wind direction: ——— 117°, – – – 122°.

Figure 30 Angle sensitivety of lateral movement around a hill in stratified flow (Snyder, 1988)

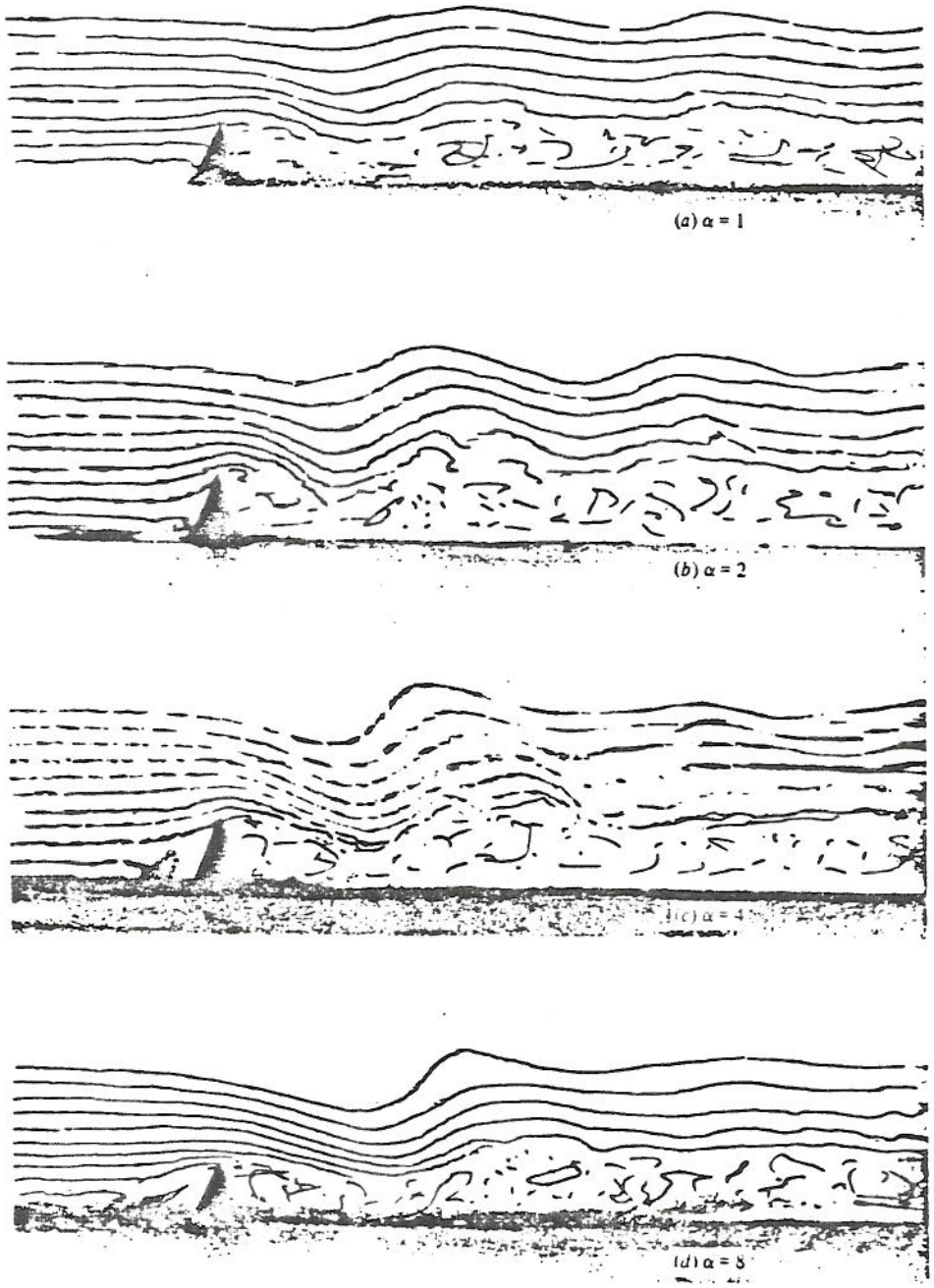

Figure 31 Dye streaks obtained during stratified tow-tank experiments of flow over triangular-shaped ridges of various aspect ratio (Castro et al., 1983)

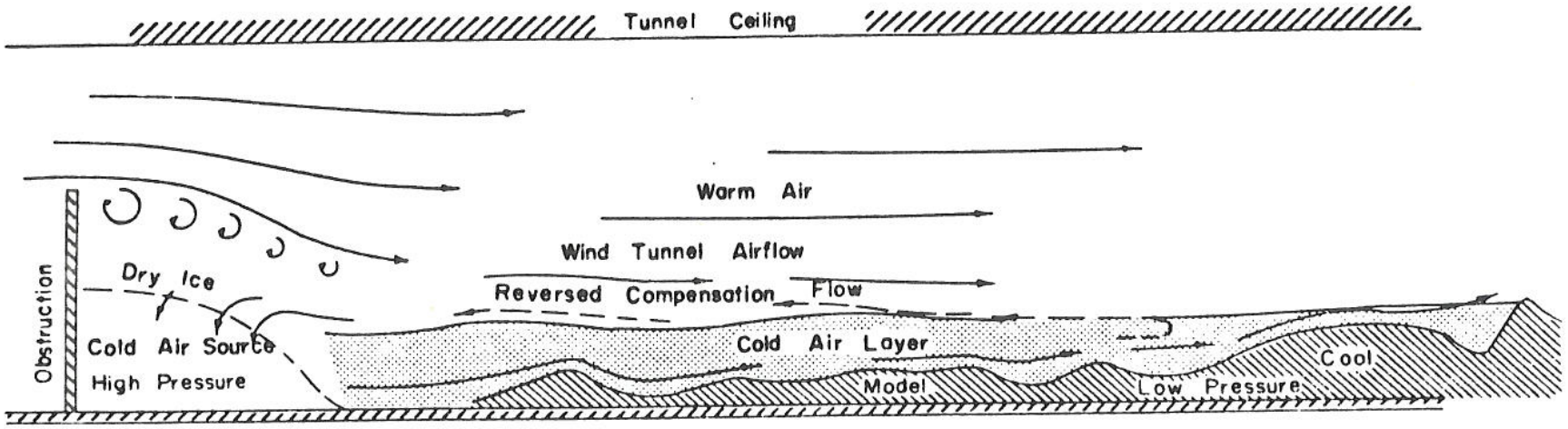

Figure 32 Schematic representation of the wind tunnel airflow from the combination of windtunnel and dry ice (Orgill et al., 1971a)

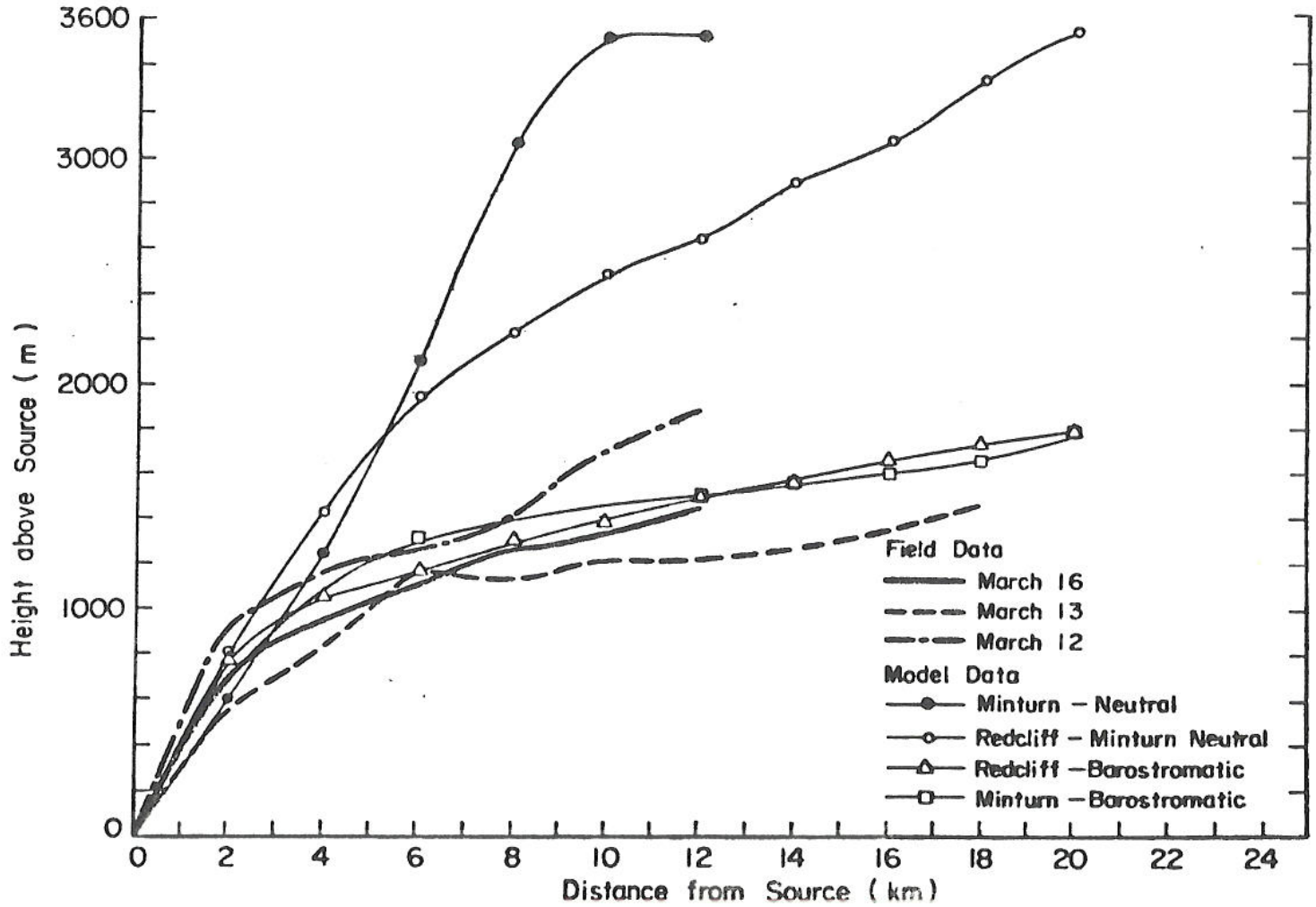

Figure 33 Comparison between the vertical rise of model and field tracer plumes during the Eagle Valley/Climax cloud seeding experiments (Orgill et al., 1971a)

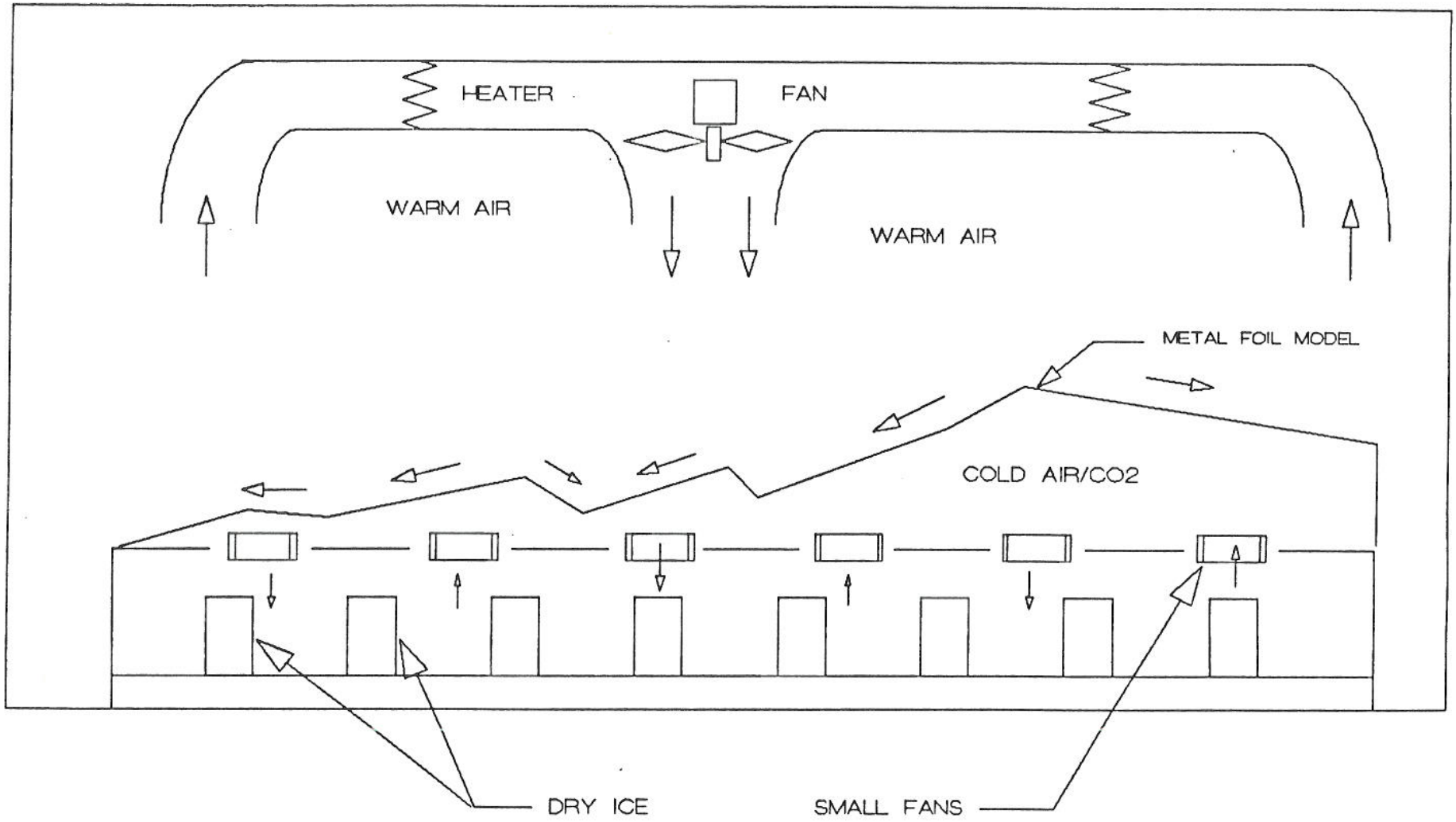

Figure 34 Schematic of convection chamber at Colorado State University used to simulate mountain-valley drainage patterns.

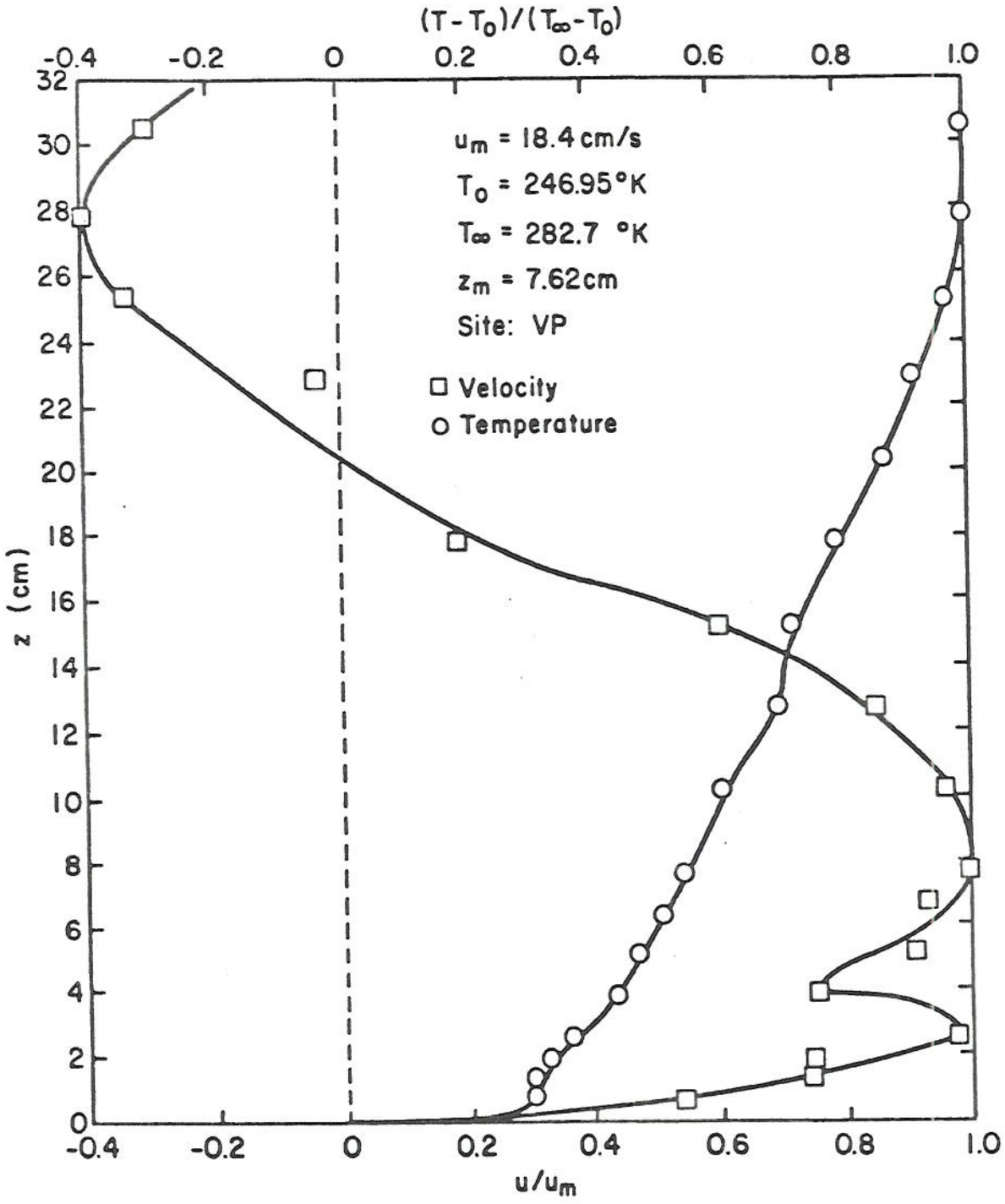

Figure 35 Velocity and temperature profiles taken over the mine site for the Coal Creek Drainage flow tests: Ri = 1.69 (Petersen and Cermak, 1980)

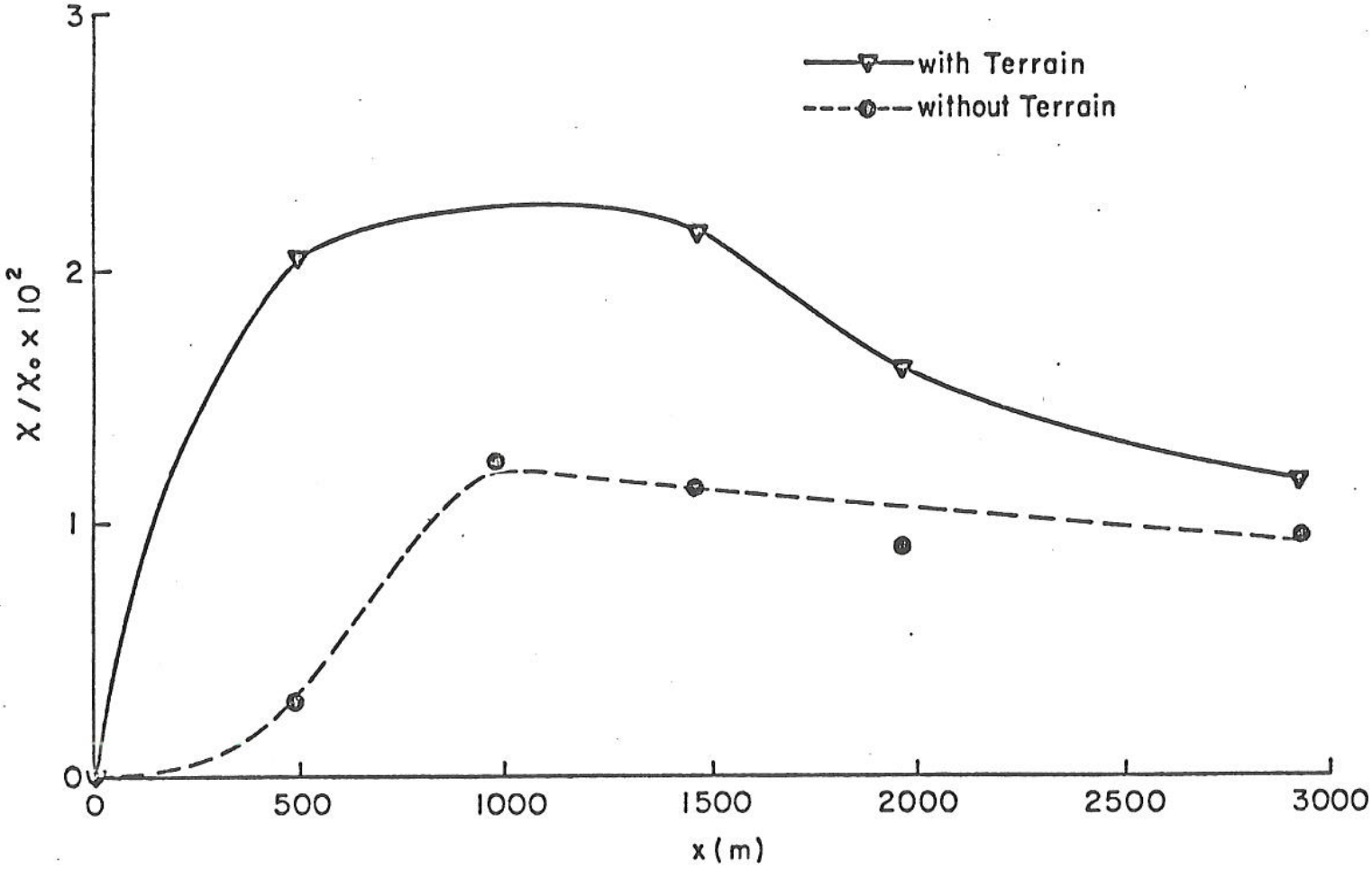

Figure 36 Maximum ground level concentrations versus downwind distance with and without model terrain for a 6.7 m/s prototype wind speed and Kingston Power Plant Units 1 through 9 operating (Graham et al., 1978)

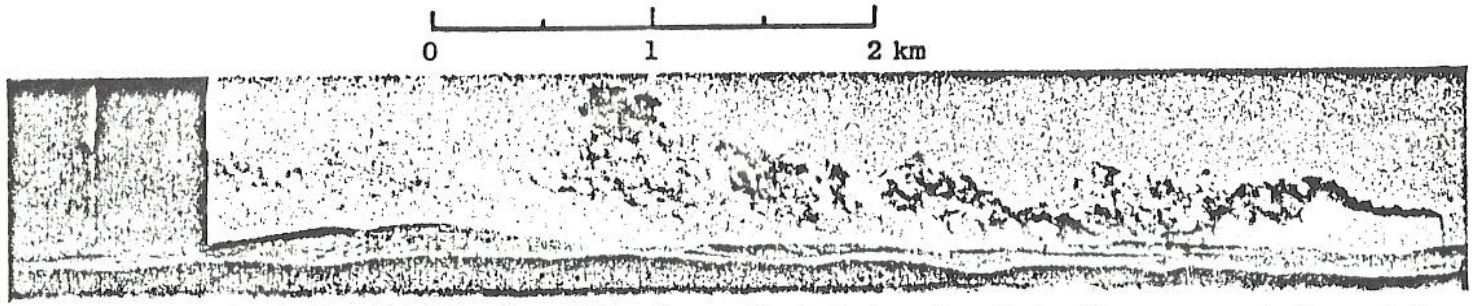

a. Run IVa: Neutral Condition, N = 0 Hz, U_∞ = 12.6 cm/s, K = 1.4, $F_H = \infty$, and F_D = 3.9

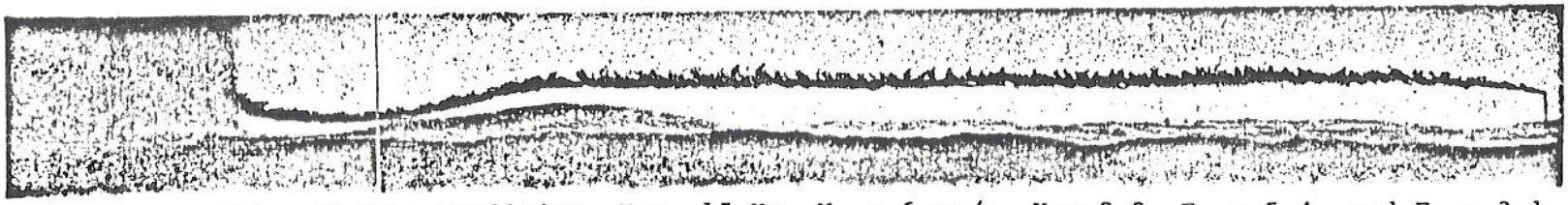

b. Run IVb: Stable Condition, N = .15 Hz, U_∞ = 6 cm/s, K = 2.2, F_H = 5.4, and F_D = 3.1

c. Run IVc: Stable Condition, N = .15 Hz, U_∞ = 3 cm/s, K = 4.4, F_H = 2.7, and F_D = 3.1

Figure 37 Plume visualization of side view of plume dispersion from a lead smelter in Glover, MO. Simulation in a stratified towing tank for neutral and stratified flows (Liu and Lin. 1985)

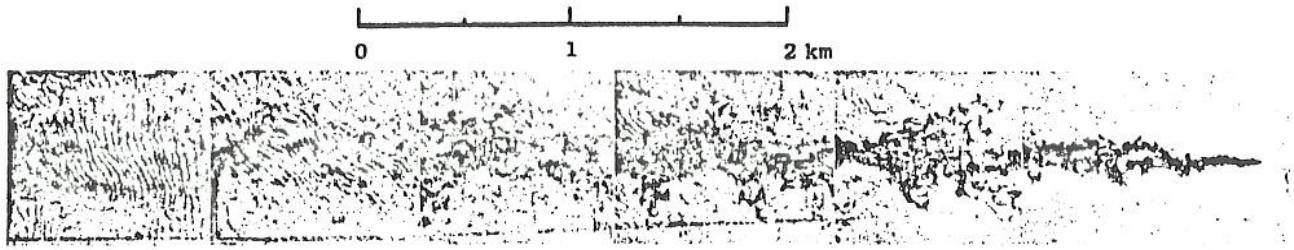

d. Run IVa: Neutral Condition, N = 0 Hz, U_∞ = 12.6 cm/s, K = 1.4, F_H = ∞, and F_D = 3.9

e. Run IVb: Stable Condition, N = .15 Hz, U_∞ = 6 cm/s, K = 2.2, F_H = 5.4, and F_D = 3.1

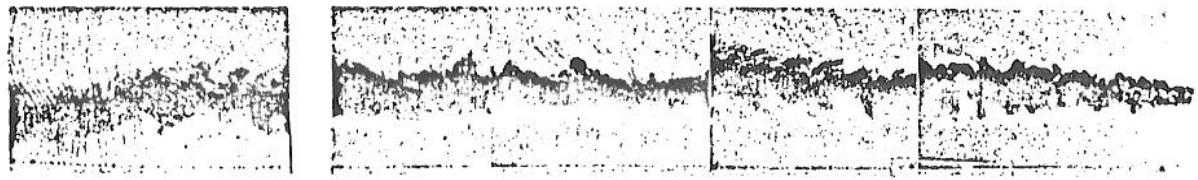

f. Run IVc: Stable Condition, N = .15 Hz, U_∞ = 3 cm/s, K = 4.4, F_H = 2.7, and F_D = 3.1

Figure 38 Plume visualization of top view of plume dispersion from a lead smelter in Glover, MO. Simulation in a stratified towing tank for neutral and stratified flows (Liu and Lin, 1975)

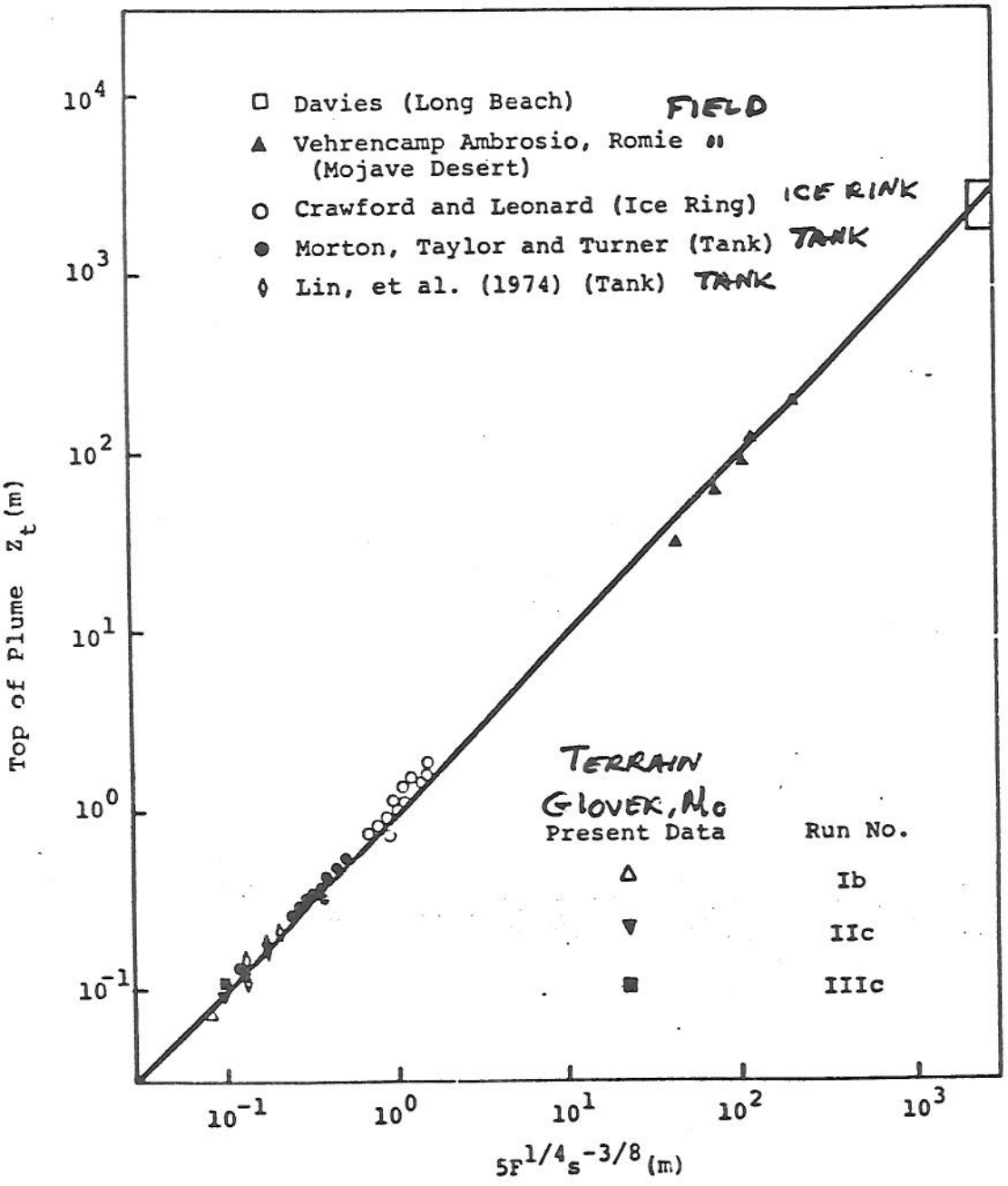

Figure 39 Laboratory and field data from Glover lead smelter plume simulation compared with field data of plume rise in calm and stable flows (Liu and Lin, 1975)